Assessment of Skeletal Muscle Microperfusion Using MRI

Sasan Partovi, Bjoern Jacobi, Yaron Gordon, Lisa Zipp, Anja-Carina Schulte, Sasan Karimi, Rolf Huegli, and Deniz Bilecen

Contents

S. Partovi · L. Zipp · A.-C. Schulte · R. Huegli · D. Bilecen (✉)
Department of Radiology and Nuclear Medicine,
University Hospital Bruderholz, Bottmingen, Switzerland
e-mail: deniz.bilecen@unibas.ch

S. Partovi
Department of Radiology,
University Hospitals Case Medical Center,
Case Western Reserve University,
Cleveland, OH, USA

B. Jacobi
Third Department of Medicine-Hematology,
Oncology, Pneumology, University Medical Center of Johannes Gutenberg-University, Mainz, Germany

Y. Gordon
Department of Diagnostic and Interventional Radiology,
University Hospital Heidelberg, Heidelberg, Germany

L. Zipp
Department of Pediatrics,
Rainbow Babies and Chidren's Hospital,
Cleveland, OH, USA

S. Karimi
Department of Neuroradiology,
Memorial Sloan-Kettering Cancer Center,
New York, NY, USA

Abstract

Blood oxygenation level-dependent (BOLD) MRI, arterial spin labeling (ASL) and dynamic contrast enhancement (DCE) are current magnetic resonance imaging (MRI) techniques allowing the non-invasive functional assessment of peripheral microvasculature in healthy and diseased individuals. The functional imaging of skeletal muscle microvasculature helps to understand muscular and vascular physiology and alterations of microcirculation under certain pathological conditions such as peripheral arterial occlusive disease, diabetes mellitus, chronic compartment syndrome and rheumatic disorders. BOLD MRI uses blood as an endogenous contrast agent provided by the different magnetic properties of oxy- and deoxyhemoglobin. The BOLD contrast in skeletal muscle tissue primarily arises from the microcirculation yielding a very sensitive tool for alterations of the physiological oxygen supply and demand. However, the complex nature of the BOLD contrast's origin also entails a variety of variables complicating the interpretation of BOLD signal changes. ASL's ability to directly measure muscle perfusion may prove to be a powerful tool for the evaluation of disease progression and the evaluation of therapies aimed at improving muscle perfusion. As is the case with BOLD MRI, this holds particularly true for patients who are unable to receive contrast agents, a collective which is often afflicted with vascular impairments. Dynamic contrast enhanced MRI may contribute considerably to objectively evaluate many musculoskeletal diseases through its ability to measure multiple microvascular properties. The potential of these three MRI methods to non-invasively assess disease severity and the efficacy of new therapeutic strategies, such as stem cell and gene therapy, renders them as very appealing future research targets.

M.-A. Weber (ed.), *Magnetic Resonance Imaging of the Skeletal Musculature*, Medical Radiology. Diagnostic Imaging,
DOI: 10.1007/174_2013_911, © Springer-Verlag Berlin Heidelberg 2013
Published Online: 20 September 2013

1 Keypoints

1. BOLD MRI of skeletal muscle tissue relies on the intravascular ratio between deoxy- and oxyhemoglobin primarily in small muscle vessels. This ratio is dependent on the microcirculatory function, small vessel perfusion, blood volume, oxygen consumption, and hemoglobin content. It is measured as $T2^*$ signal in gradient echo MR sequences.
2. The muscle BOLD MRI signal is influenced by a variety of factors, among them are age, weight, physical activity, examined muscle fiber type, and the intake of vasoactive drugs.
3. Muscle BOLD MRI requires special paradigms for provoking an adequate signal which can be analyzed quantitatively. Three paradigms are currently used in the clinical arena: Arterial occlusion to provoke ischemia and reactive hyperemia, muscle exercise, and oxygen inhalation.
4. Muscle BOLD MRI shows significant differences in the $T2^*$ time course and key parameters between healthy volunteers and patients with peripheral arterial occlusive disease, chronic compartment syndrome, diabetes mellitus, or rheumatic disease, such as systemic sclerosis and granulomatosis with polyangiitis (also known as Wegener's granulomatosis).
5. ASL utilizes the selective excitement (tagging) of inflowing blood spins into a tissue of interest. Without the use of contrast agents and applying specially designed radiofrequency pulses, the inflowing tagged spins induce a measurable change in the apparent tissue $T1$, which is directly used to calculate local perfusion.
6. DCE-MRI investigates the tissues intensity response to an intravenously injected bolus of contrast agent over a period of time. By applying compartmental models to the data obtained, microvascular properties, such as fractional volumes of plasma and blood, vessel permeability and perfusion can be obtained.

2 Part 1 Skeletal Muscle BOLD MRI

2.1 General Principles of BOLD MRI

2.1.1 The BOLD Effect in Muscle Tissue

The oxygenation level of intravascular hemoglobin can be used for the assessment of muscular microcirculation (i.e., arterioles, capillaries, and venules) in magnetic resonance imaging (MRI) because of its influence on the static magnetic field (Jacobi et al. 2012). This method is called blood oxygenation level-dependent (BOLD) MRI and is derived from functional MRI of the human brain where it has been applied since the early 1990s (Ogawa et al. 1990a).

The BOLD signal is based on the principle that the hemoglobin iron ion without a coordinated oxygen molecule has unpaired electrons in its atomic shell which render deoxyhemoglobin paramagnetic. That means that deoxyhemoglobin leads to changes of the magnetic susceptibility of water protons in the vessel surrounding, whereas diamagnetic oxyhemoglobin does not (Thulborn et al. 1982; Ogawa et al. 1990b). The result is a dropout of $T2/T2^*$ weighted MR signal with an increasing ratio between intravascular deoxy- and oxyhemoglobin. Initially, this effect has been used to map functional active brain regions (Bandettini et al. 1992; Ogawa et al. 1992). In these regions, neuronal activation is accompanied by a paradoxically larger increase of local microperfusion than of neuronal oxygen consumption, an observation first made in 1986 (Fox and Raichle 1986). This coupling of neuronal activity and microperfusion results in an increase of the ratio between capillary and venous oxy- and deoxyhemoglobin, resulting in a decrease of paramagnetic species and hence a positive BOLD signal. The understanding of the main functional origin of the BOLD effect has led to a broad application of BOLD studies in functional brain imaging (Fig. 1) (Partovi et al. 2012a, e). But owing to the diverse physical and physiological factors influencing the BOLD signal in the brain, this field is still under investigation (Logothetis and Wandell 2004).

Similar to neuronal tissue, skeletal muscles offer pronounced alterations of microvascular blood flow depending on the degree of resistance vessel vasodilatation (Boushel et al. 2000). During muscular activity, local arteriolar smooth muscle contraction is mainly reduced via local mediators such as pCO_2, H^+/lactate, K^+, adenosine, NO, and recently discovered myokines such as IL-6, IL-8, and IL-15 (Sarelius and Pohl 2010; Pedersen et al. 2007). The first attempts to use these large functional variations of muscular perfusion in BOLD MR imaging were performed in the late 1990s.

In one study, an arterial occlusion paradigm (see *Paradigms and related time courses*) was applied to show that the $T2^*$ signal in a gradient echo sequence decreases during ischemia and shows a fast surge to a pronounced peak approximately 30 s after reactive hyperemia (Toussaint et al. 1996). Both effects were mainly attributed to the susceptibility effect of deoxyhemoglobin on protons in the vessel surrounding already known from BOLD studies of the human brain. This hypothesis was strengthened by the finding that mean $\Delta R2$ correlated well with perfusion as measured indirectly by MR plethysmography during reactive hyperemia. Another study from this early muscle BOLD era further supported the fact that hemoglobin oxygenation is mainly responsible for the $T2^*$ signal since the desaturation of muscle myoglobin—as measured with MR spectroscopy—started later and slower when compared

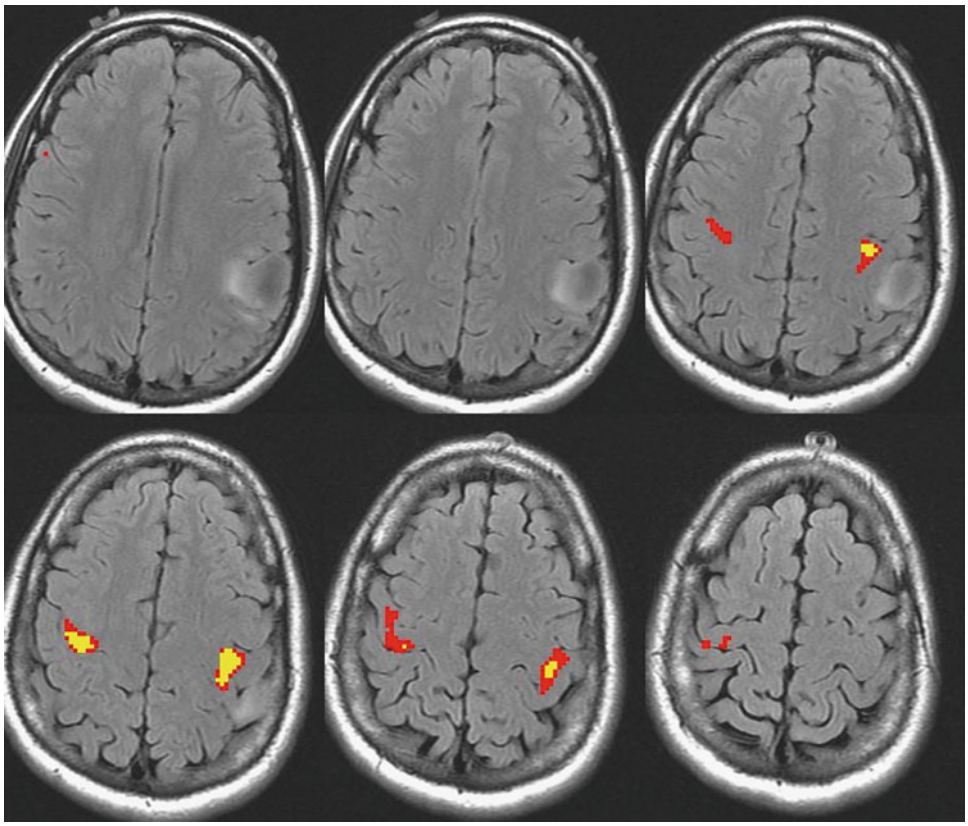

Fig. 1 BOLD MRI of the brain showing activation in motor gyrus as response to a finger tapping task. BOLD imaging in this patient with a low grade glioma was performed preoperatively for surgical planning

with the $T2^*$ signal dropout during ischemia (Lebon et al. 1998a). Given the strong functional relationship between neuronal activity and BOLD signal changes in the human brain, it is quite interesting that first comparable studies, investigating the physiological relationship between muscle contraction and $T2^*$ signal changes, were not undertaken until the beginning of the early 2000s. In a first report, specific transient $T2^*$ signal boosts were discovered in the calf after short 3 s lasting isometric muscle tension exercises with the gastrocnemius or soleus muscles (see *Paradigms and related time courses*) (Hennig et al. 2000). Interestingly, those muscular hemodynamic responses bared similar inherent time constants when compared with neuronal tissue, indicating a possible common coupling mechanism between oxygen demand and blood supply in both tissues. Another study using a comparable exercise paradigm with short muscle contractions demonstrated a good temporal correlation between stimulation induced BOLD signal surges and hemoglobin saturation as measured by near infrared spectrometry (NIRS) (Meyer et al. 2004). This correlation could even be clarified in a recent work by Towse et al. showing that hemoglobin oxygenation plays a major role in muscle BOLD signal changes, depending primarily on perfusion and blood volume (Towse et al. 2011). They proposed that—at least with regard to exercise paradigms—muscle activity induces an increase of blood volume in the local microcirculation that, depending on hemoglobin's oxygenation status, lead to a positive (in case of an increase of the oxy- to deoxyhemoglobin ratio) or negative (in case of a decrease of the oxy- to deoxyhemoglobin ratio) BOLD response.

These major determinants of the BOLD effect in skeletal muscle, i.e., hemoglobin oxygenation, perfusion, and blood volume, have also been found to play a pivotal role with regard to arterial occlusion paradigms. The increase of muscle perfusion—as measured by arterial spin labeling (ASL)—has been shown to be strongly associated with BOLD signal peaking (Duteil et al. 2006). This effect was closely dependent from the venous filling state, with extensive venous filling producing a larger BOLD response. The muscular BOLD response has also been compared with standard clinical diagnostic tools for the assessment of tissue perfusion (i.e., laser Doppler flowmetry, LDF) and oxygenation (i.e., transcutaneous oxygen pressure measurement, $TcPO_2$) (Ledermann et al. 2006a). Although LDF and $TcPO_2$ measurements are limited to superficial skin layers and do not measure perfusion or oxygenation changes in the muscle tissue, the BOLD signal in the calf muscles was closely correlated with blood flow and oxygenati on during ischemia and reactive hyperemia.

In the case that perfusion and volume dependent hemoglobin oxygenation changes are the main source of the

BOLD effect in skeletal muscle, one would expect that primarily intravascular relaxation effects are responsible for the measured $T2^*$ changes in muscle tissue. According to experimental data and numerical simulations from the last decade this is indeed the case (Meyer et al. 2004; Sanchez et al. 2010). Sanchez et al. were able to eliminate $T2^*$ changes induced by arterial occlusion using an inversion-recovery sequence to null the arterial signal, showing that a significant extravascular contribution to the bulk muscle BOLD contrast could be ruled out (Sanchez et al. 2010).

Taken together, the current evidence of skeletal muscle BOLD MRI supports a model, in which alterations of muscle perfusion lead to blood volume changes that—depending on the oxygenation status of hemoglobin—increase or decrease the $T2^*$ signal. Of course, further work will need to be done to fully understand the mechanisms yielding a BOLD response in muscle tissue. It has to be taken into account that the qualitative and especially the quantitative influence of each physiological parameter on the BOLD signal might change under different experimental conditions and imaging paradigms. However, as the skeletal muscle tissue represents the "end organ" of the peripheral vasculature, BOLD MRI is a promising and evolving imaging method for the functional evaluation of vascular diseases, such as peripheral arterial occlusive disease (PAOD), diabetes mellitus, compartment syndrome, and the majority of rheumatic diseases (Partovi et al. 2012b).

2.1.2 Technical Fundamentals of BOLD MRI

BOLD MRI of skeletal muscles is usually performed in whole body MRI scanners with magnetic field strengths ranging between 1.5 and 4 T. Consecutively, it is possible to analyze every muscle within the body, but—with regard to accessibility for cuff compression and typical clinical questions—usually arm or leg muscles are imaged. Regardless of the paradigm used, it is crucial to place the individual on the MR examiner couch for 10–15 min prior to the beginning of the examination to prevent extensive filling of venous vessels that will impact the results (Duteil et al. 2006).

As oxygenation changes appear in a short time frame, BOLD imaging needs high-speed acquisition methods. These are generally based on echo-planar imaging (EPI) (Howseman and Bowtell 1999). BOLD signal alterations of conventional single-shot EPI are sensitive to changes in $T2^*$ and $T2$—reflecting oxygenation—and initial BOLD signal intensity (S_0). S_0 is influenced by several confounding parameters such as blood inflow, changes in $T1$, and baseline drifts (Speck and Hennig 1998; Schulte et al. 2001). With Multi-echo gradient-echo EPI sequences it is possible to isolate oxygenation-related changes ($T2^*$) from these other effects (Ledermann et al. 2006b; Schulte et al. 2008). With each excitation, images at different effective echo times usually ranging between 7 and 80 ms are acquired (Jacobi et al. 2012; Ledermann et al. 2006b; Kos et al. 2009). Acquisition parameters have to be adjusted to the short $T2^*$ (<20 ms) in skeletal muscle.

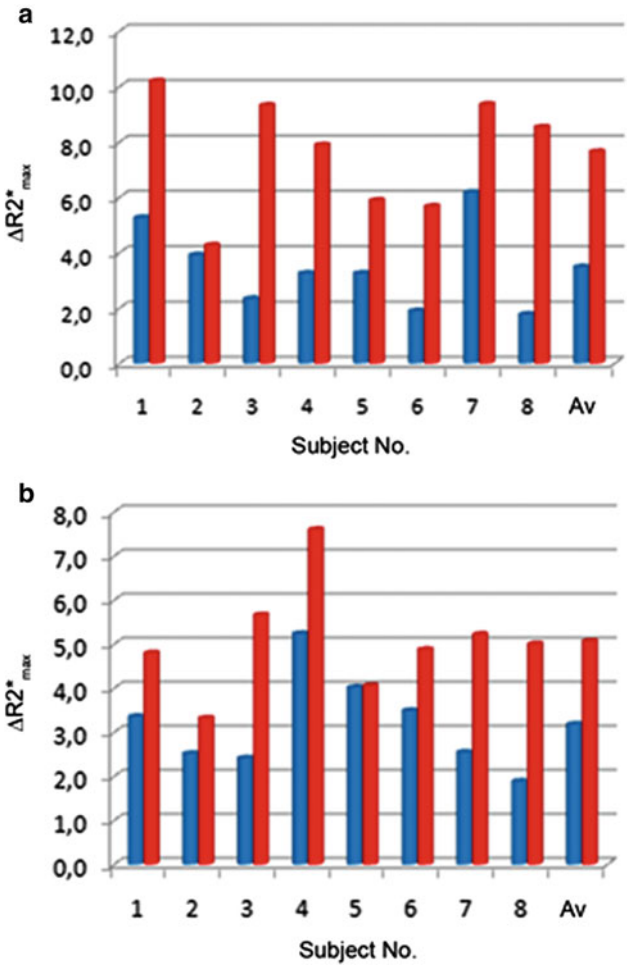

Fig. 2 $\Delta R2^*$max values at 1.5 T (*blue*) and 3.0 T (*red*) BOLD MRI of soleus **a** and gastrocnemius **b** muscle in each of the eight examined volunteers. From Partovi et al. (2012c). This material is reproduced with permission of John Wiley and Sons, Inc

Several studies have shown that the magnetic field strength has a significant impact on the extent of $R2^*$ changes in skeletal muscle in both, arterial occlusion and exercise paradigms (Meyer et al. 2004; Lebon et al. 1998b; Partovi et al. 2012c). Partovi et al. directly analyzed the relation between $\Delta R2^*$ and the magnetic field (B_0) strength using 1.5 and 3.0 T whole body scanners (Partovi et al. 2012c). This study showed a nearly proportional relationship between B_0 and $\Delta R2^*$, being in good concordance with previous studies evaluating this relationship in the human brain (Fig. 2) (Turner 1997; Gati et al. 1997; Van der Zwaag et al. 2009).

Spin echo sequences ($T2$) may also be applicable for BOLD imaging but offer a bad temporal resolution.

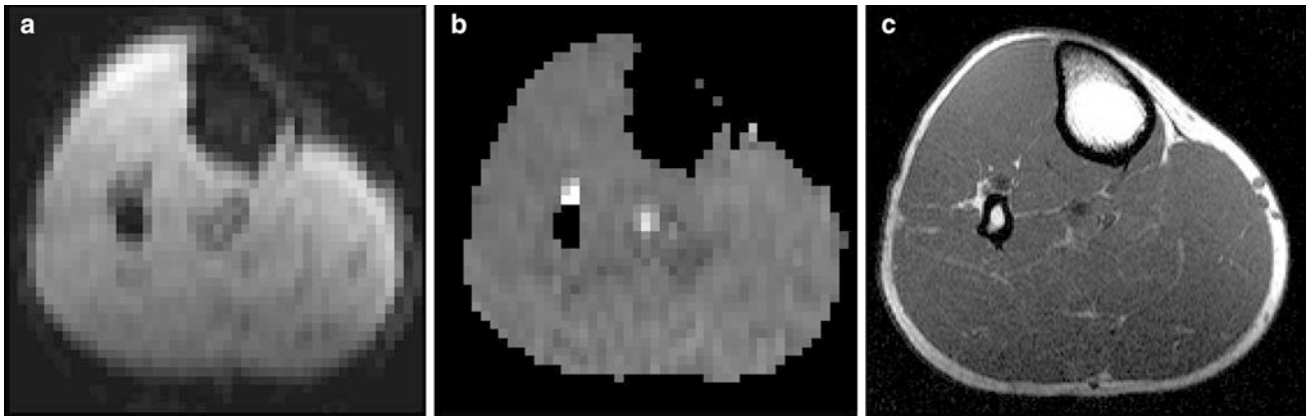

Fig. 3 Echo-planar-imaging (**a**), $T2^*$ map (**b**) and T*1* anatomical reference image (**c**) of a healthy 34-year-old volunteer showing the upper region of the left calf. Anatomical reference is used to map ROIs in the $T2^*$ maps and to exclude visible vessels which could influence the BOLD signal

Additionally, gradient echo sequences emphasize local magnetic field distortions induced by paramagnetic species such as deoxyhemoglobin. To facilitate and improve the placement of the ROIs on *T*2* maps calculated from the EPI data, *T*1-weighted images of the same layers should also be obtained. With regard to the placement of regions of interest (ROI) for extracting the $T2^*$ dataset, this enables avoidance of visible vessels from the BOLD measurement to minimize inflow artifacts (Fig. 3).

2.1.3 Paradigms and Related Time Courses

BOLD imaging of skeletal muscles is based on the principle of temporal changes in the ratio between oxy- and deoxyhemoglobin inside skeletal muscle microvessels, that lead to an endogenous contrast in $T2/T2^*$ MR sequences. To provoke measurable BOLD signal alterations in skeletal muscles, different imaging paradigms have been developed. The most often applied paradigms are arterial occlusion (= cuff compression), muscle exercise, and oxygen inhalation.

Arterial occlusion is probably the most often applied imaging paradigm in skeletal muscle BOLD MRI. This may be due to its early implementation at the beginning of the evaluation of BOLD MRI in skeletal muscle tissue and several advantages when compared with other BOLD muscle MRI settings (Toussaint et al. 1996; Lebon et al. 1998a). Arterial occlusion contains a simple experimental setup, in which a standard air cuff is wrapped around the mid-thigh or upper arm of the examined extremity (Fig. 4). If the device consists of ferromagnetic parts, a safe distance from the magnet should be achieved by using an extended tube. Fast (automated) inflation of the air cuff to an occlusion pressure at least 50 mmHg above the individual systolic blood pressure is needed to induce complete ischemia and, on the other hand, minimize the discomfort of patients with vascular disease and reduce their risk of exacerbating critical limb ischemia. Medial calcific sclerosis

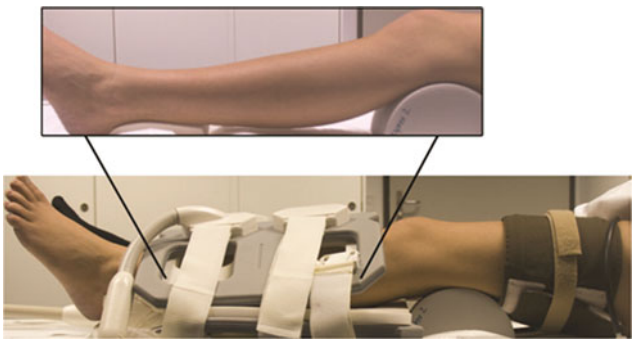

Fig. 4 Experimental setup of an arterial occlusion paradigm including two flexible array coils and sphygmomanometer wrapped around the thigh of the investigated leg. The cuff was additionally fixed with a velcro strap. The lower leg was supported at knee and foot level (insert) to prevent compression of the calf muscles. From Jacobi et al. (2012). This material is reproduced with permission of John Wiley and Sons, Inc

(Mönckeberg's arthrosclerosis) should be considered if higher cuff pressures are needed to achieve full ischemic conditions, especially in patients with diabetes. MR measurements are usually started during resting state (reflecting baseline), ischemia and during reactive hyperemia after cuff deflation till reaching baseline level. The most important advantage of this paradigm for skeletal muscle BOLD MRI is the induction of profound oxygenation changes and a consecutively excellent BOLD contrast. Furthermore, this paradigm is independent from patient compliance, it can be standardized in the clinical setting and motion artifacts—as known from BOLD imaging of the brain or exercise paradigms in muscle tissue—are reduced to a minimum. The BOLD signal time courses extracted from studies with arterial occlusion paradigms typically show a faster initial $T2^*$ signal decay at the beginning of ischemia followed by a slower decrease to a minimum ischemic value (MIV, $T2^*_{min}$) (Fig. 5). After cuff deflation, a fast surge of the

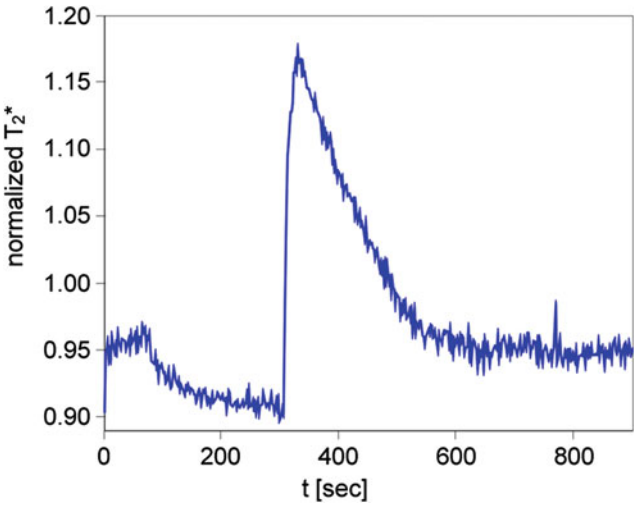

Fig. 5 Typical BOLD $T2^*$ time course extracted from a 30-year-old male healthy volunteer during an arterial occlusion paradigm showing the typical signal decrease during a 3 min lasting ischemia period and a $T2^*$ surge after cuff deflation with subsequent hyperemia peaking after approximately 40 s (TTP)

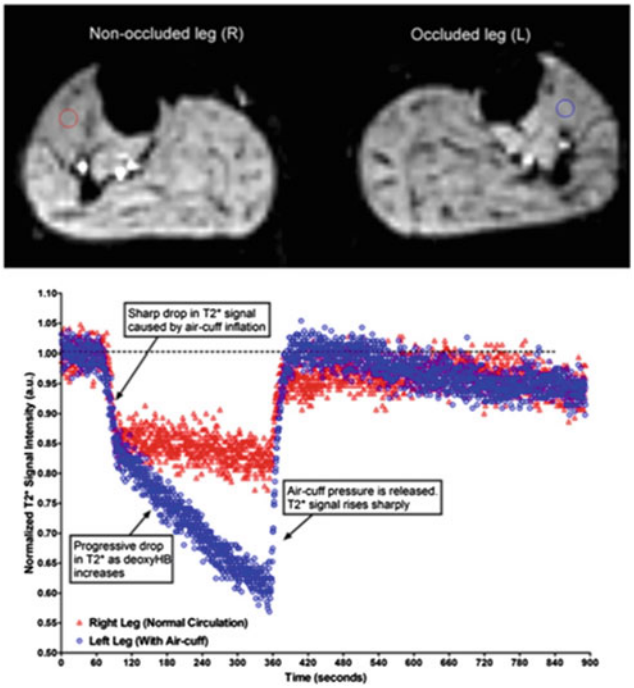

Fig. 6 $T2^*$ dynamic images (*upper panel*) acquired from both legs of a healthy female volunteer with corresponding ROIs (left leg: *blue;* right leg: *red*). Ischemia was only induced at the left leg. An aberrant fast initial $T2^*$ signal drop could be detected in the left tibialis anterior muscle. The similar pattern was also detected in the non-occluded right leg. From Yeung et al. (2012). This material is reproduced with permission of John Wiley and Sons, Inc

BOLD signal is observed with peak values (HPV, $T2^*_{max}$) after approximately 30–60 s (Time to peak, TTP) and a subsequent decrease to a steady state value around baseline. A recent study performed with a lower limb phantom and healthy volunteers revealed that compressed oxygen from an air cuff can induce magnetic susceptibility changes leading to a fast decline of the $T2^*$ signal (Yeung et al. 2012). This $T2^*$ signal dropout proofed to be pressure-dependent and could also be localized in the contralateral leg of the examined volunteers, where the blood flow was not interrupted (Fig. 6). These interesting results call for a critical reevaluation of the described fast initial signal dropouts during the ischemia phase of arterial occlusion studies. Furthermore it has to be evaluated, if cuff position can be optimized or special inflation gases without effects on magnetic susceptibility, such as nitrogen, need to be used in this setting in the future.

Muscle exercise paradigms have also been applied in a variety of muscle BOLD studies. They take advantage of the physiological coupling between muscle contraction and local perfusion. It has been shown that brief isometric contractions of only 1 s are sufficient to evoke measurable BOLD responses (Hennig et al. 2000; Meyer et al. 2004). The peaking of such responses follows approximately 8 s after each contraction induced motion artifact and the baseline value is reached again after 10–15 s (Meyer et al. 2004). Those BOLD responses have been proven to be dependent on the muscle contraction intensity (Wigmore et al. 2004). Although being the most "physiological" of the usually applied paradigms in skeletal muscle BOLD imaging, voluntary muscle contractions are largely dependent on patient compliance. Thus, standardization in the clinical setting seems to be challenging. Motion artifacts are a further drawback and require the use of specific fixation devices.

Oxygen inhalation has been used to provoke a BOLD signal increase of skeletal muscle (O_2-enhanced MRI) (Noseworthy et al. 1999, 2003). Prior to MR imaging, the individual breathes 100 % oxygen for several minutes to increase the amount of dissolved O_2 of the blood. As arterial hemoglobin is nearly completely saturated with oxygen under normal conditions, it has been proposed that the BOLD response of muscle tissue in oxygen inhalation paradigms is primarily increased via an oxygen uptake by venous deoxyhemoglobin (Noseworthy et al. 2003). However, O_2 itself is paramagnetic and leads to changes of $T1$, $T2$, and $T2^*$. Studies using this paradigm should thus be analyzed with care regarding true BOLD effects that depend on hemoglobin oxygenation (Partovi et al. 2012b).

2.1.4 Important Parameters Influencing Muscle BOLD Signal

Different parameters have been shown to have a certain influence on the $T2/T2^*$ signal of skeletal muscles. The most prominent role among those factors play age, weight, physical activity, examined muscle fiber type, intake of

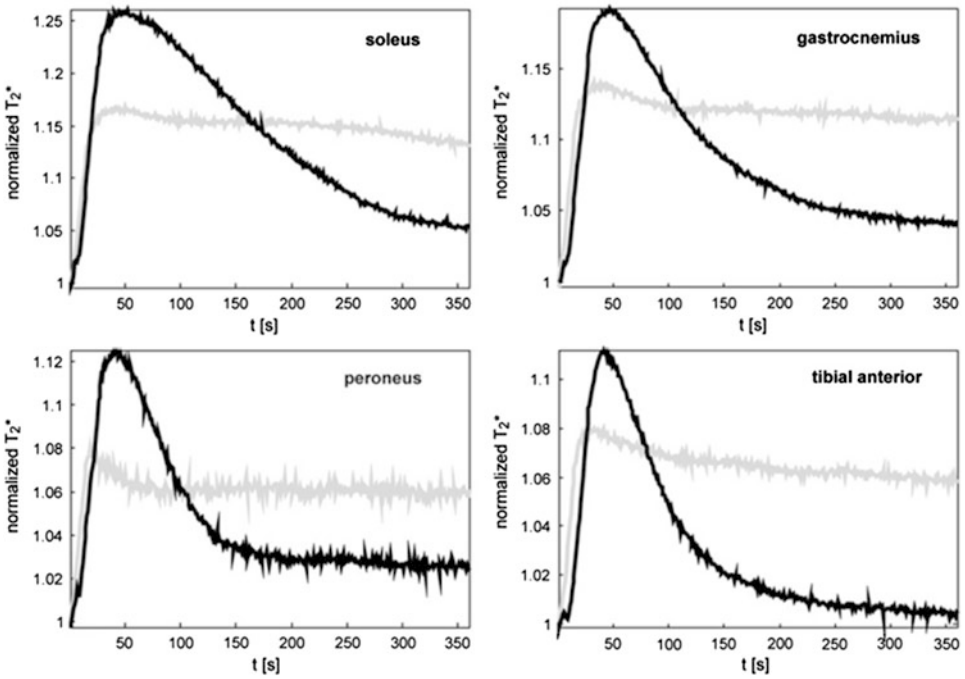

Fig. 7 Mean BOLD responses of four investigated calf muscles during 360 s of reactive hyperemia in elderly healthy subjects (*gray lines*) and young healthy subjects (*black lines*). Note, the significantly lower $T2^*$ hyperemia peak value ($P = 0.005$) and significantly elevated $T2^*$ end value ($P < 0.001$) in the elderly group compared with the younger individuals. From Schulte et al. (2008). This material is reproduced with permission of Radiological Society of North America (RSNA)

vasoactive drugs, and Hb-content, some of which will be further discussed in this section. Regardless of performing skeletal muscle BOLD studies in a preclinical or clinical setting it is crucial to take these parameters into account since they may possibly confound the results.

Aging leads to specific structural and functional impairments of skeletal muscle vasculature that result in an increased vascular rigidity and decreased perfusion reserve (Muller-Delp 2006; Proctor et al. 2003). Those alterations might explain the BOLD $T2^*_{max}$ and TTP reduction found in elderly volunteers (mean age 64.0 years ± 6.4, $n = 11$) after cuff induced reactive hyperemia when compared with younger subjects (mean age 30.3 years ± 6.5, $n = 17$) (Schulte et al. 2008). However, due to the missing correlation with methods enabling to investigate the relationship to blood volume, perfusion, or oxygenation, the authors could only speculate with regard to the noticeable elevated end value after 350 s of hyperemia in the older study collective (Fig. 7). During cuff induced ischemia, a significant reduction of $T2^*_{min}$ and delay of the $T2^*$ decrease (Time to reach half ischemic minimum, THIM) has been described in the elderly (Kos et al. 2009). Interestingly, this ischemia BOLD pattern does not match the alterations found in patients with peripheral arterial occlusive disease (PAOD, see *Clinical applications*), indicating that further mechanisms beside atherosclerosis play a role in vascular aging.

Increased body weight is associated with vascular dysfunction and decreased vasodilatation reserve (Gu and Xu 2013). For this reason, it is not surprising that the BOLD response of skeletal muscle tissue is also compromised in obese patients when compared with lean people. However, this effect could only be detected at a level of significance in one of the examined muscles (extensor digitorum longus), at maximum voluntary contractions and a short TE of 6 ms, primarily reflecting blood volume changes (Sanchez et al. 2011).

Slow-twitch oxidative muscles (i.e., soleus, tibialis anterior) show a higher capillary density and myoglobin content than fast-twitch glycolytic muscles (i.e., gastrocnemius, extensor digitorum longus) (Noseworthy et al. 2003; Zierath and Hawley 2004). Consecutively, the largest BOLD responses are usually detected in slow-twitch muscles, whereas smaller changes are typically found in fast-twitch muscles (Ledermann et al. 2006b; Noseworthy et al. 2003; Donahue et al. 1998). Regarding the high oxygen sensitivity of BOLD MRI and the interindividual variation of absolute $T2^*$ values, the selection of the optimal muscle type to investigate is crucial to obtain significant results when assessing patient and control collectives.

With regard to the activity level, individuals reporting to participate in aerobic sports greater than 30 min per day for at least 5 days a week bear an up to threefold larger BOLD signal increase when compared with sedentary individuals reporting no regular physical activity (Towse et al. 2005, 2011). The relation of constant physical activity to the oxygenation status of skeletal muscle microcirculation may obviously be explained by vascular adaptations such as increased capillary density, collateral blood flow, and exercise-provoked vasodilation (Green et al. 2011, 2012). Thus, it will be helpful to control for the physical activity level in muscle BOLD studies, for example by using an adapted questionnaire. Furthermore, even brief exercising

over several minutes prior to BOLD imaging induces a remarkable $T2^*$ increase in the exercised muscles and thus has to be avoided in clinical settings (Bulte et al. 2006).

Especially in (pre)clinical muscle BOLD studies with patient collectives suffering from vascular diseases, the intake of vasoactive drugs might be a problem which has to be taken into account. As the BOLD response has been shown to be primarily dependent on perfusion induced blood volume and oxygenation changes, drugs affecting the vasodilatation capacity will influence the measured BOLD signal changes. Indeed it has been demonstrated that drugs inducing vasodilatation significantly increased oxygen- and ischemia-induced BOLD responses, whereas vasoconstrictors significantly reduced $\Delta T2^*$ (Bulte et al. 2006; Utz et al. 2005).

2.2 Clinical Applications of BOLD MRI

2.2.1 Peripheral Arterial Occlusive Disease

The morphological correlate of peripheral arterial occlusive disease (PAOD) is stenoses and occlusions in peripheral arteries leading to impaired blood supply to the end organs, such as the muscular system and the skin. Symptoms ranging from claudication to gangrene are the sequela of these morphological changes. Stenoses on the arterial level can be detected non-invasively with magnetic resonance angiography (Prince 1998; Rofsky and Adelman 2000) or color-encoded doppler ultrasonography (Leng et al. 1991). In a couple of studies muscle BOLD MRI proved to be useful for non-invasive assessment of PAOD. In one of the earlier studies BOLD MRI during the hyperemic phase using the arterial occlusion paradigm has been investigated in PAOD patients versus an age-matched healthy volunteer group. Despite inducing ischemia by cuff compression followed by hyperemia after pressure release, the paradigm was well tolerated with minor discomfort in the patient group. In comparison to the healthy volunteers the BOLD time course in PAOD patients showed a decreased $T2^*_{max}$ and a delayed TTP (Fig. 8) (Ledermann et al. 2006b). The lower $T2^*_{max}$ might be caused by a slower flow of blood through the muscle microvasculature resulting in efficient deoxygenation of hemoglobin and by a rarefaction of capillaries in the calf muscle as a result of the disease as it was found in previous studies (Hickey et al. 1992; Dawson and Hudlicka 1990). The delayed TTP might be based on impaired flow of oxygenated blood into the microcirculatory system of the calf muscle (Lebon et al. 1998a). Besides a relationship between TTP and the ankle brachial pressure index could be demonstrated; with some exceptions a lower ankle brachial pressure index was associated with a higher TTP (Ledermann et al. 2006b). Muscle BOLD MRI investigations during the ischemic phase in PAOD patients

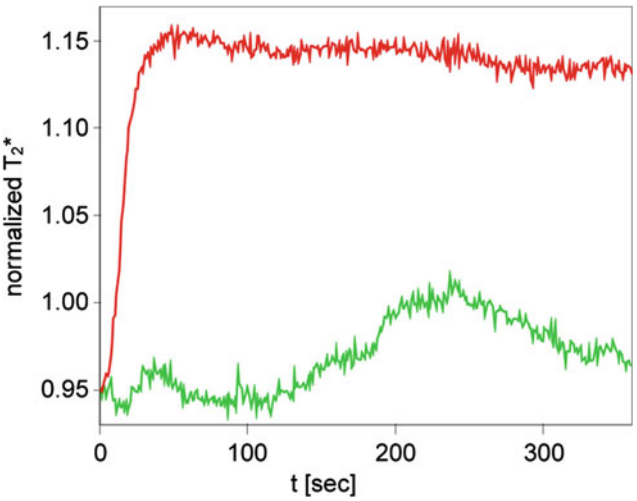

Fig. 8 BOLD $T2^*$ signal changes of a male PAOD patient (stage IIA) during reactive hyperemia is shown in *green*. For comparison, a normal $T2^*$ time course of a healthy 67-year-old female volunteer is shown in *red*. Pay attention to the profoundly decreased $T2^*$ recovery during reactive hyperemia with no obvious peak in the patient with PAOD

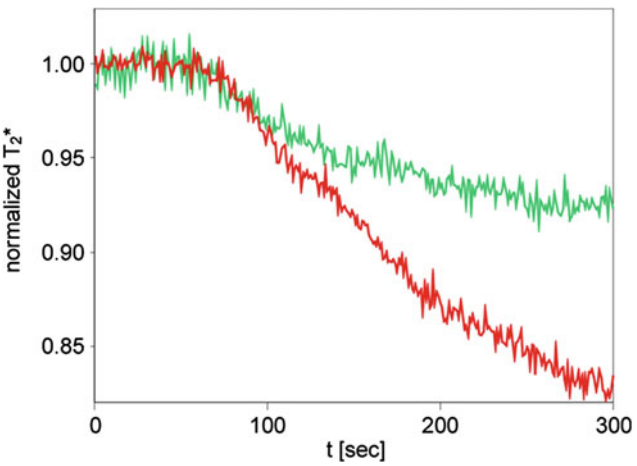

Fig. 9 $T2^*$ time course of a 36-year-old female PAOD patient (stage IIa, *green line*) with a marked reduction of $T2^*$ decline during ischemia. In *red*, a normal $T2^*$ time course of a healthy 52-year-old male is shown with a substantially lower MIV at the end of ischemia

have been published as well. A significant altered $T2^*$ time course in comparison to an age-matched healthy volunteer group was found (Potthast et al. 2009). The $T2^*_{min}$ was lower in the PAOD group versus the non-PAOD group (Fig. 9).

The BOLD sequence as part of a multiparametric MR imaging protocol is highly interesting for therapy response evaluation. A study monitored PAOD patients longitudinally 1 day before and 6 weeks after percutaneous transluminal angioplasty (PTA) performing muscle BOLD MRI. The arterial occlusion paradigm was well tolerated in this

PAOD patient population as well, proving the feasibility of the innovative technique (Huegli et al. 2009). The cuff compression paradigm is advantageous for clinical use as it does not require compliance and its standardization is easier than an exercise based approach (Berglund and Eklund 1981). It can be safely applied in PAOD patients with intermittent claudication. However, those with higher grade of the disease (critical limb ischemia or necrosis) were not enrolled in previously published studies because of a theoretical risk of exacerbation when ischemia is provoked in the early phase of the paradigm (Huegli et al. 2009). After PTA $T2^*_{max}$ increased, whereas TTP and EV decreased but these changes in BOLD key parameters did not reach statistical significance. However, they demonstrated a trend resulting in reversal of the BOLD response towards a normal healthy course. Post PTA $T2^*_{max}$ increase can be explained by improved blood supply and TTP decrease might be based on a more effective and faster flow through the re-opened superficial femoral arteries. Another reason for the higher $T2^*_{max}$ is an improved vasodilatation reserve after percutaneous intervention. The decreased EV found in this study might be explained by a fast washout of oxygenated blood from the musculature.

A recently published study analyzed the reproducibility of imaging techniques for the assessment of the macro- and microcirculatory network in a PAOD patient collective in comparison to a healthy volunteer group. The evaluation of the microcirculation included dynamic BOLD imaging during the hyperemic phase performing the arterial occlusion paradigm. For BOLD imaging reproducibility was not demonstrated. In detail the key parameter relative $T2^*_{max}$ revealed poor reproducibility, whereas TTP showed moderate reproducibility (Versluis et al. 2011). Further studies with a standardized paradigm and imaging parameters are warranted to improve the reliability of the BOLD response. A potential alternative to muscle BOLD MRI for assessment of PAOD is contrast-enhanced ultrasound. A recently published study on healthy volunteers used an arterial occlusion paradigm for muscle perfusion quantification performing contrast-enhanced ultrasound. The arterial occlusion paradigm can be applied in patient populations, such as in subjects with PAOD for the evaluation of skeletal muscle microperfusion (Krix et al. 2011). Another study also showed that contrast-enhanced ultrasound is able to diagnose PAOD by detecting skeletal muscle microperfusion and arterial perfusion reserve alterations (Amarteifio et al. 2011).

2.2.2 Rheumatic Disorders

The skeletal muscle tissue is the functional end organ of the peripheral vascular system. In patients with rheumatic disorders BOLD MRI has the potential to contribute to non-invasive evaluation of the clinically relevant microcirculatory system disorders. Furthermore, in those patients with symptoms of the musculoskeletal system muscle BOLD MRI may even elucidate the cause as subclinical microcirculatory alterations.

In a recently published case study a female patient with a history of granulomatosis with polyangiitis (also known as Wegener's granulomatosis) presented with bilateral severe myalgia (Jacobi et al 2013). The patient had no signs of atherosclerotic disease and no associated risk factor for macrovascular compromise. Morphological MR with $T2$ weighted images did not reveal any signs of inflammation explaining the symptoms of the patient. However, BOLD MRI could demonstrate pronounced impairment of calf muscle microcirculation. In comparison to the BOLD signal time course of a matched healthy volunteer substantial differences in key parameters were shown: The $T2^*_{min}$ was decreased and the declining slope during ischemia was increased in the patient. The lower MIV might be explained by small vessel vasculitis leading to a larger amount of oxygen consumption.

Investigations of the BOLD response in systemic sclerosis (SSc) patients generated interesting results. SSc is a disease with microangiopathy leading to insufficiency in a variety of tissues (Gabrielli et al. 2009). Up to one-third of patients have symptoms in the musculoskeletal system (Walker et al. 2007). In a study the microvasculature of SSc patients was analyzed performing BOLD imaging of the calf muscle with the arterial occlusion paradigm. Impaired muscle microcirculation was demonstrated by altered BOLD time courses in the patients compared to a healthy volunteer control group (Partovi et al. 2012d). Key parameters were significantly different with lower $T2^*_{max}$, $T2^*_{min}$, declining slope values and a prolonged TTP. Lower $T2^*_{min}$ might be based on rarefaction of capillary or occlusion of the microcirculatory system. The hyperemia parameter differences might be the result of structural (capillary loss or obliteration) or functional (vasoconstrictor effect or decreased vasodilatation reserve) vasculopathy. BOLD response alterations have been found to be more pronounced in the gastrocnemius than the soleus muscle in this study. A further study with SSc patients tried to elucidate the origin of altered muscle BOLD MR time courses by means of correlation with transcutaneous oxygen pressure (TcPO2) measurements. TcPO2 is a technique utilizing the modified Clark electrodes and reflecting the tissue oxygenation status (Bunt and Holloway 1996; Slagsvold et al. 1992). A comparison with healthy volunteers was included in the analysis as well. Very strong cross correlations between both imaging techniques in the patient and healthy volunteer group were demonstrated for a time lag of approximately 40 s (Partovi et al 2013). This proves BOLD MRI as a valuable tool for the assessment of patients with SSc as it reveals oxygen deficits in this patient population.

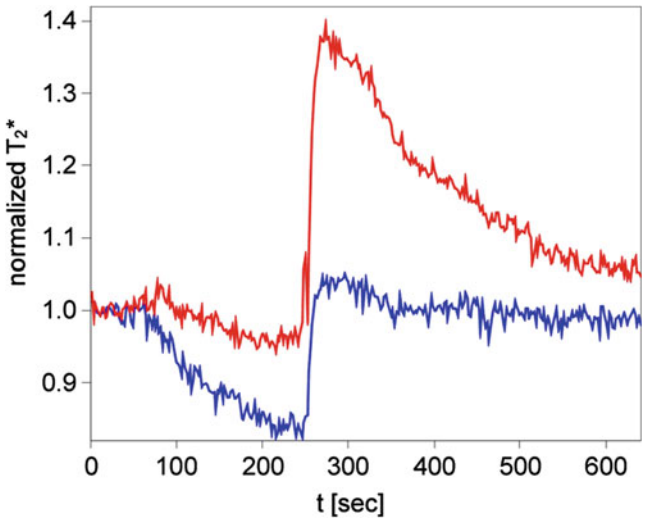

Fig. 10 BOLD time courses of a 53-year-old male SSc patient (*blue*) and a 26-year-old healthy female volunteer (*red*) showing a clear reduction of $T2^*_{min}$ and $T2^*_{max}$ in this rheumatic disorder

The origin of the $T2^*$ signal of BOLD MRI can be explained at least partially by tissue oxygenation alterations. When comparing the signal course of both modalities, the $T2^*$ decrease was more pronounced than the decrease of the TcPO2 signal during ischemia. From a pathophysiological standpoint this lower signal might be caused by the adaption of the microcirculatory system to chronic hypoxia leading to a pronounced capillary oxygen consumption. $T2^*_{max}$ and the TcPO2 signal were lower in the patient population versus healthy volunteers which is based on either structural or functional vasculopathy as discussed above. In the future vasoactive drugs might help to further clarify whether the structural or the functional component contributed to the BOLD response or if both components impact the signal to a certain degree (Bulte et al. 2006). Furthermore muscle BOLD MRI correlations in SSc patients with laser Doppler flowmetry are of interest (Fagrell 1986; Ranft et al. 1986) (Fig. 10).

2.2.3 Diabetes Mellitus

It is well known from a clinical perspective that the microvasculature is impaired in patients with diabetes mellitus type I and type II (Picchi et al. 2010; Marcovecchio and Chiarelli 2011). Muscle BOLD MRI was assessed in patient with diabetes mellitus type I and II versus healthy controls conducting maximal isometric ankle dorsiflexion for 1 s (muscle exercise) as paradigm. The authors of this study also evaluated the distal macrovasculature with phase contract MR angiography. No significant differences in the BOLD response between patients and healthy controls could be found. There was also no different in the findings from phase contract MR angiography. This study could confirm the impact of age on the BOLD signal time course (Slade et al. 2011). Combining BOLD with a technique to assess macrovasculature is a promising approach towards functional musculoskeletal imaging.

For assessing the microvasculature of the skeletal muscle in patients with diabetes mellitus contrast-enhanced ultrasound could be an interesting imaging modality. Contrast-enhanced ultrasound in patients with diabetes mellitus type II performing the arterial occlusion paradigm revealed impaired skeletal muscle microperfusion in comparison to healthy volunteers (Amarteifio et al 2013).

2.2.4 Compartment Syndrome

For certain applications it was suggested to integrate muscle BOLD MRI and other advanced MR techniques in one imaging protocol. For instance BOLD MRI can be combined with diffusion tensor imaging which enables depiction of muscle tears. In the same publication BOLD MRI was demonstrated to be feasible for the detection of vascular insufficiency in compartment syndrome (Noseworthy et al. 2010).

3 Part 2 Arterial Spin Labeling MRI

3.1 General Principles of ASL

3.1.1 Origin of the ASL Signal

The principal underlying ASL is the selective visualization of fresh inflowing blood into a tissue of interest which can be imaged with this technique. This is achieved by magnetically labeling (or "tagging") of inflowing arterial blood water proximal of the tissue of interest, generally through inversion or saturation of the longitudinal magnetization using specifically designed radiofrequency (RF) pulses (Detre et al. 1992).

The water molecules, acting as an endogenous contrast agents and carrying the labeled magnetization, travel through the vascular tree to a particular tissue where they are extracted from the microvascular bed and join the larger pool of tissue water distal of the tagging location. Once arriving in the tissue, after a duration termed arterial transit time, the tagged spins induce a measurable change in the apparent tissue $T1$ signal and in the tissue magnetization, which it is detected by a conventional MR sequence. To produce a control image, the experiment is then repeated without the labeling procedure. Consecutively, the image signals are subtracted in pairs to yield a difference of signal, which enables detection of tagged blood that was delivered to the imaging slice (Fig. 11). This signal directly reflects quantitative local perfusion which is calculated using modifications in the original Bloch equations.

However, the tagging sequence produces additional static signals in the tissue to be imaged (a process termed

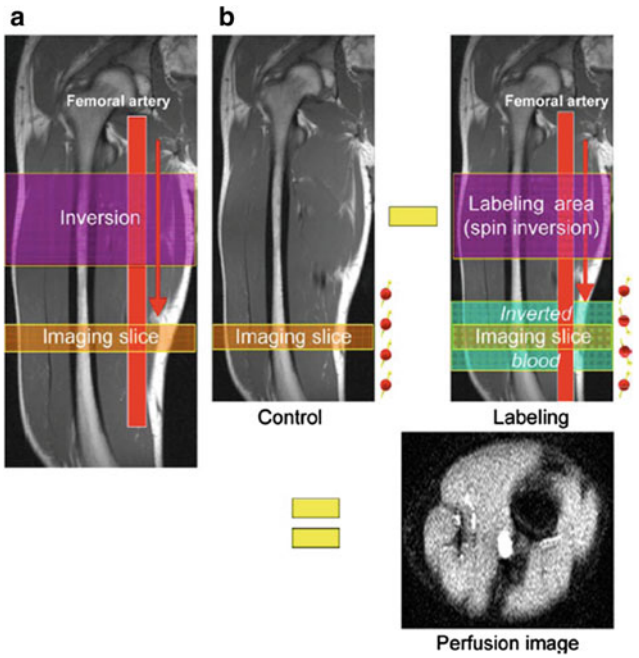

Fig. 11 Principle of ASL MR perfusion imaging. **a** In ASL MRI, blood serves as intrinsic contrast agent. For this, blood is magnetically labeled by an inversion pulse outside the imaging slice and then flows, depending on the blood flow, into the imaging slice. **b** The difference between the MR image with and the MR image without labeled blood yields an image with signal only from inflowing blood, whereas background signal is suppressed. This image is the perfusion weighted ASL image. From Weber et al. (2007). This material is reproduced with permission of Springer

magnetization transfer), and therefore the control sequence must produce an identical signal without labeling the inflowing blood. Provided that the off-resonance and magnetization transfer effects of the tagged and control pulses are equal, the ASL signal is simply proportional to the difference in longitudinal magnetization in the tissue due to the blood that entered the voxel during the defined time interval. The goal of all the ASL techniques is to produce a tagged image and a non-tagged control image in which the static tissue signals are the same.

The essential problem in quantifying the ASL signal is to estimate how much the magnetization of the tagged spins has decayed by the time of measurement, so that the measured ASL signal can be appropriately scaled to represent a quantity of blood delivered to the voxel (Buxton et al. 1998).

For each ASL method, a detailed model of the process combining kinetics and relaxation is needed in order to extract a quantitative measurement of perfusion. Although all of these models rely on the same theoretical background one should take into account that each ASL technique uses different types of parameter values. These parameters include: the degree of arterial spin inversion, transit time from the labeling slice to the imaging slice, $T1$ of blood and tissue, equilibrium magnetization of arterial blood, clearance of magnetization by venous flow, blood-tissue partition coefficient for water, duration of the labeling pulse, and the amount of blood water extracted by the tissue. These parameters are subsequently used in equations describing perfusion which are derived from the modified Bloch equation.

It should be considered that the ASL calculation of perfusion is not derived from dynamic datasets and does not require deconvolution processing. The ASL signal is directly and linearly proportional to perfusion.

3.1.2 Advantages and Disadvantages of ASL

The main advantage of ASL lies in its complete non-invasive assessment of perfusion and microcirculation. This permits serial measurements without the need for administration of contrast agents. ASL is quantitative in absolute terms and evaluates the actual tissue microperfusion as opposed to blood flow to an organ. The information derived from BOLD imaging can be acquired partially when applying the ASL technique (Duteil et al. 2006; Carlier et al. 2006). Additionally, ASL exhibits relatively high spatial and high temporal resolution. Finally, ASL may be used to conduct non-invasive MR angiography (Katoh et al. 2008; Rehwald et al. 2004; Wheaton and Miyazaki 2012).

The greatest disadvantage of ASL is the intrinsic low signal-to-noise ratio (SNR). The difference in signal between the two images is approximately 1 %, thus multiple images are acquired (consisting of repeats of tag minus control image) which are then averaged. This process is time consuming and makes low perfusion states (such as muscle perfusion at rest) more difficult to quantify, although not impossible.

Since its first demonstration by Detre et al. (1992) and Kwong et al. (1992), ASL has been applied extensively to studies of the brain (Detre et al. 1999; Chalela et al. 2000; Alsop et al. 2000), the heart (Troalen et al. 2013; Kober et al. 2004; Zhang et al. 2005) as well as other organs (such as the kidneys and lungs) (Robson et al 2012; Mai and Berr 1999) including the skeletal muscle (see section below and Fig. 12).

3.1.3 Sources of Error and Artifacts Associated with ASL

Motion Artifacts: Due to the lengthy acquisitions to achieve adequate SNR, as well as the fact that ASL perfusion imaging involves the subtraction of two images with an intensity almost 100 times larger than the difference between them, ASL scans are susceptible to motion artifacts. Recent technical advances offer several solutions to the problem (Norris and Schwarzbauer 1999; Wong et al. 2006; Frouin et al. 2006; Garcia et al. 2005; Ye et al. 2000; Blamire and Styles 2000; Duyn et al. 2001).

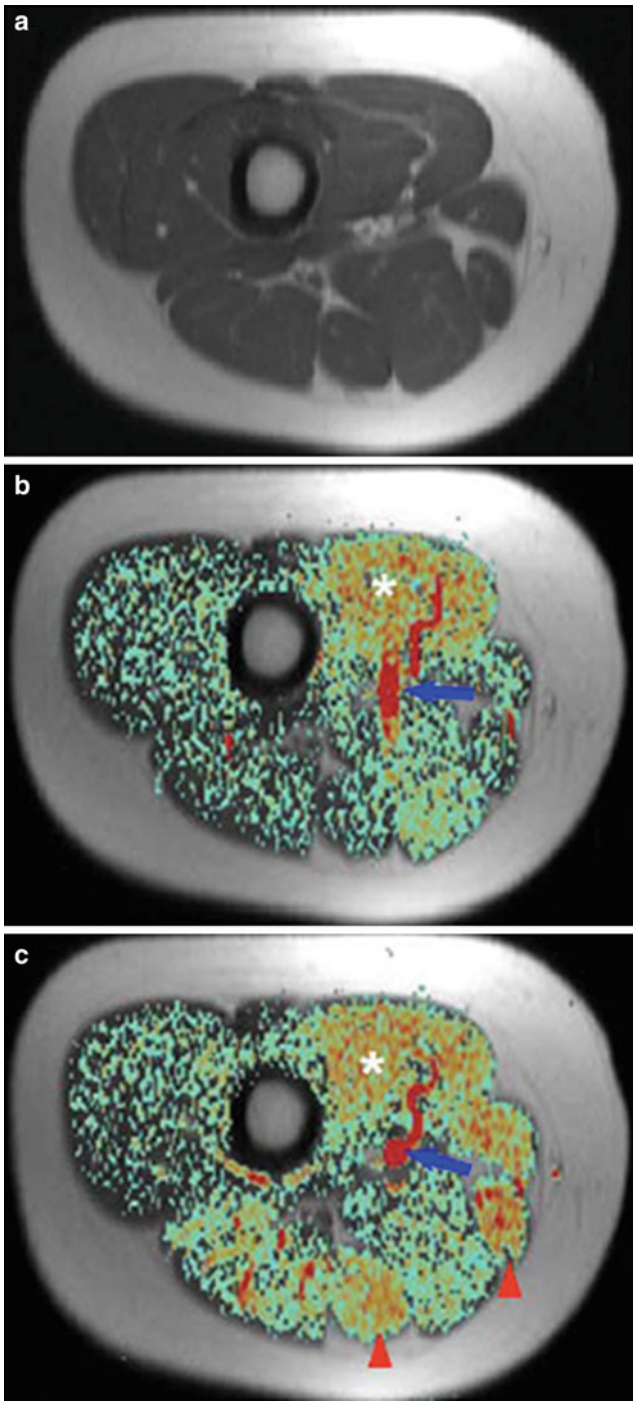

Fig. 12 Anatomic *T*1-weighted image (**a**) and color-coded perfusion weighted ASL image (**b**) of the right mid-thigh of a 24-year-old woman at rest on a 1.5-T whole body scanner (PICORE tagging scheme, 10-mm slice thickness, $TR = 3{,}500$ ms, $TE = 30$ ms, inflow time $TI = 600$ ms, 256–128 matrix, 25 averages, acquisition time $TA = 3$ min). After knee flexion exercise against a 3-kg weight for 5 min significant hyper-perfusion in all thigh-flexor muscles can be observed (*arrowheads*), while the adductor muscles (*asterisk*) already have elevated perfusion at rest-resulting from a preceding exercise test (**c**). The *blue arrow* indicates the femoral vessels, which have the highest signal on ASL images. As expected, no perfusion signal appears in bones and subcutaneous fat tissue. From Weber et al. (2007). This material is reproduced with permission of Springer

Magnetization Transfer (Discussed Above): Magnetization transfer effects can be a significant source of error in ASL measurements. They can be particularly problematic in skeletal muscle, where magnetization transfer rates are relatively high (Niemi et al. 1992) and can change significantly and rapidly during exercise (Mattila et al. 1993; Zhu et al. 1992).

Post Labeling Transit Time Delay: The exact duration of the transit time is challenging to determine as it is not uniform across a slice or between slices. The artifact results from intravascular labeling that has not yet reached capillaries and tissue by the time the image the acquisition is carried out. As a consequence perfusion might be underestimated.

Alsop and Detre reduced the sensitivity of the continuous ASL techniques to transit time heterogeneity by inserting a postlabeling delay (PLD) (Alsop and Detre 1996). However, this approach still requires a good estimation of the transit time since the optimal delay time equals the transit time. This makes the approach difficult to implement in skeletal muscle where arterial flow velocities can be expected to change considerably between rest and exercise (Wu et al. 2008).

Contribution of Labeled Water in Large Vessels: Intravascular tagged blood flowing through the slice creates large focal intensities, which are unrelated to tissue perfusion. In practice, the signal from large arteries is typically destroyed in the course of the echo-planar imaging acquisition without the need of additional bipolar gradients (Buxton et al. 1998). To further reduce this artifact another possibility is to carefully exclude voxels containing vessels or lipids (which cause large focal intensities as well).

Incomplete Inversion of the Arterial Blood (Labeling Efficiency): In the skeletal muscle blood flow velocity can range from very low to very high levels, potentially resulting in different labeling efficiencies.

Venous Outflow Effect: An implicit assumption in most existing quantitative perfusion models is that the tagged blood does not leave the tissue prior to data acquisition. In situations involving high flow rate this might not hold true. It is particularly important to consider this in investigations in the skeletal muscle, where fast flow rates are encountered as well as conditions associated with low hematocrit levels such as anemia (Wu et al. 2008). Insufficient consideration of these artifacts will result in perfusion estimation errors.

3.2 Technical Principles

According to the tagging scheme, ASL can be divided into four categories: continuous ASL (CASL), pulsed ASL (PASL), pseudo-continuous ASL (pCASL), and alternative labeling schemes.

3.2.1 Continuous ASL

With CASL techniques, the blood is continuously labeled. A spatially localized RF field, positioned through the feeding arteries of the tissue of interest, inverts the longitudinal magnetization of the protons in the blood as they flow through a thin slice. This technique uses long RF pulses. The original scheme proposed only allows quantification of perfusion in a single slice (Detre et al. 1992). This problem was overcome when a new CASL techniques was developed in order to quantify regional cerebral blood flow in multiple slices with a single coil (Alsop and Detre 1998; Talagala et al. 1998).

3.2.2 Pulsed ASL

As opposed to labeling blood as it flows through a plane, PASL relies on the instantaneous labeling of a thick slice (large blood volume) with a short RF pulse (~10–20 ms). PASL sequences are based on a scheme originally referred to as flow-sensitive alternating inversion recovery (FAIR) sequences (Kwong et al. 1995; Kim 1995; Schwarzbauer et al. 1996). In FAIR, an inversion-recovery sequence is performed twice—a labeled one with slice-selective inversion and a control one with nonselective inversion. Following each inversion imaging is performed. The inversion-recovery image with the slice-selective inversion pulse is then subtracted from the image with the nonselective inversion pulse (Fig. 13).

3.2.3 Pseudo-Continuous ASL Techniques

pCASL is a novel labeling scheme that combines the advantages of PASL and CASL (Silva and Kim 1999). The advantages of pCASL include an increase of 50 % in SNR as compared to PASL and a higher tagging efficiency than CASL (Wu et al. 2007). pCASL measurement sequences are available on MR systems of all three major vendors.

3.2.4 PASL versus CASL

Whereas pCASL and PASL can be implemented with standard MR-systems, CASL requires a dedicated coil with a capacity for generating continuous RF pulses (Wu et al. 2011). PASL is performed with shorter repetition times and thus leads to superior temporal resolution (Wong et al. 1998). PASL is also less sensitive to variations in the assumed or measured values of the tissue parameters. BOLD data can be acquired simultaneously with PASL. PASL exhibits lower influence of magnetization transfer (Boss et al. 2006) and inversion efficiency is higher and thus essentially flow-velocity independent.

For PASL, the inherent SNR is lower than that of CASL. However, when tagging efficiency and coil configuration are considered, the SNR is comparable between PASL and CASL and is highest with pCASL (Wu et al. 2011). In addition, CASL techniques are less susceptible to motion

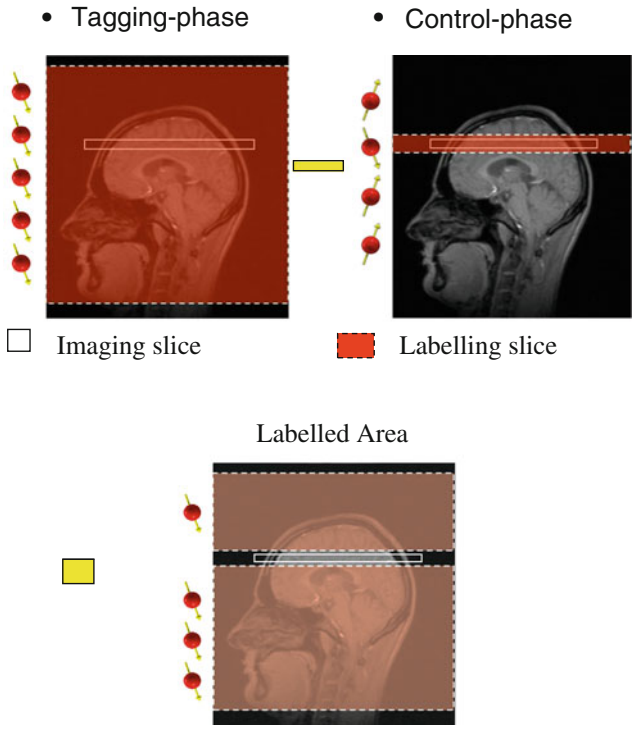

Fig. 13 Principal of FAIR (flow-sensitive alternating inversion recovery). During the tagging phase all the spins in the tagging slice are inverted. Following this, only the spins in the imaging slice are inverted (*white box*). The difference between the intensity of the imaging slice at both these times delivers the signal, which is used to calculate the blood flow. From Weber et al. (2004). This material is reproduced with permission of Springer

interferences (Wong et al. 1998; Frank et al. 1999; Richardson et al. 2001).

3.2.5 Skeletal Muscle ASL

The first ASL measurements of muscle perfusion date back to 1996 (Toussaint et al. 1996). The authors used a CASL-NMR model originally developed by Detre et al. (1992). for the brain, to measure perfusion in the calf muscle of human volunteers during rest, ischemia, and reactive hyperemia. The authors correlated the results successfully with NMR plethysmography and were able to observe significantly different perfusion rates in the various muscle groups.

Flow-Driven Arterial Water Stimulation with Elimination of Tissue Signal

FAWSETS was the first ASL sequence introduced to specifically quantify muscle perfusion (Marro 1997; Marro et al. 2005a). FAWSETS, a CASL technique, differs from other CASL techniques in that the label consists of flow-driven adiabatic excitation rather than saturation or inversion of the arterial water. The technique offers several advantages: It eliminates the need to compensate for magnetization transfer and also for arterial transit time effects. Furthermore, it provides an improvement in time resolution

in the range of factor 2. Alas, FAWSETS can only eliminate arterial transit times in a single slice. FAWSTES was conducted in several studies to investigate perfusion in the hind limb of rats (Marro et al. 2005a, b), combining FAWSTES with ^{31}P MR spectroscopy (though not simultaneously) in order to investigate local perfusion and metabolic demand.

Another manuscript presented a further CASL sequence designed to specifically quantify muscle perfusion (Frank et al. 1999) using a standard 1.5-*T* clinical imaging system fitted with a local gradient self-designed knee coil. The authors applied a modified version of continuous ASL to demonstrate spatially and temporally resolved perfusion images of exercising human skeletal muscle (Alsop and Detre 1996). They were able to demonstrate the spatial heterogeneity of perfusion values within the various muscle groups of the lower leg and perfusion sensitivity to muscle workload. In this manuscript a method for eliminating the most serious sources of error in the measurement of muscle perfusion with ASL was demonstrated as well (Alsop and Detre 1996). This technique was combined later with ^{31}P chemical shift (CSI) imaging to compare metabolic demand and perfusion response to exercise (Richardson et al. 2001).

Saturation Inversion Recovery

The first PASL sequence for the purpose of specifically quantifying muscle perfusion was SATIR (Raynaud et al. 2001). SATIR offers the following advantages: The calculation of perfusion using SATIR is independent of possible *T*2 variations, which are known to increase in exercising muscles, and of $T2^*$ making it insensitive to the BOLD effect. SATIR is highly temporal efficient, displaying a high perfusion contrast per unit of time. The new sequence was utilized to conduct multiple experiments in various setups, combining multiple interleaved additional measurements (termed multiparametric functional-NMR) to study muscle physiology both at rest and at activity (Duteil et al. 2004, 2006; Gerontol et al. 2009; Baligand et al. 2011; Bertoldi et al. 2006; Ménard et al. 2010).

3.2.6 Comparison of ASL and BOLD MRI for Muscle Perfusion

Superiority of ASL

1. BOLD contrast is of a multifactorial nature. While ASL provides a direct absolute measurement of perfusion changes, $T2^*$ weighted BOLD MRI measures the local increases in oxygenation. This should be taken into account when interpreting BOLD information.
2. The vascular network architecture in skeletal muscle, with a preferential alignment along fibers, may induce an angular dependence of BOLD relative to the Bo field.
3. ASL is less susceptible to artifacts arising from large draining veins.
4. The exercising muscle induces an intrinsic *T*2 increase which can be a confounding effect in BOLD signal interpretation.
5. BOLD response tends to plateau at high perfusion rates (Duteil et al. 2006).
6. ASL perfusion contrast is based on longitudinal magnetization, and as such it is insensitive to bulk susceptibility effects which may impact BOLD studies (Detre and Alsop 1999).
7. In conditions where angiogenesis is stimulated, associated changes in tissue vascular fractional volume could affect BOLD response to a greater extent than vasodilation itself, thus obscuring the evaluation of the skeletal muscle vasodilatory capacity (Carlier et al. 2006).

Superiority of BOLD

1. The major advantage that BOLD has over ASL is that while a typical BOLD signal is 2 % of the raw image intensity, a typical baseline ALS signal (control-tag) is only 1 % of the raw image intensity. Although the change in ASL signal can be relatively high, this still represents only 1 % of the raw image intensity. Signal averaging can compensate for this drawback of ASL but requires an increase in scan time which limits spatial and/or temporal resolution (Lebon et al. 1998c).
2. ASL temporal resolution is limited by the need to obtain two images (tag and control). Additionally, because of the time required to allow for tagged blood to flow into the imaging slice, even multislice ASL is limited in its maximum rate of image acquisition relative to BOLD.
3. ASL requires a large number of additional measurements or assumptions, which can result in the generation of subsequent significant errors.
4. BOLD signal can be increased using high magnetic field strengths (Partovi et al. 2012c). Higher magnetic field strengths are gaining an increasing interest in the clinical arena of musculoskeletal imaging.
5. Spin echo BOLD imaging has the advantage of minimizing large vessel contributions. Moreover, it can be extracted from the same series of ASL spin echo images, which are acquired for perfusion quantification.
6. ASL suffers from a greater sensitivity to movement in comparison to BOLD MRI.

3.3 Clinical Applications of ASL

3.3.1 Recent Human ASL Studies

ASL measurements for examining perfusion in multiple human extremities was first recently performed performed

(Wu et al. 2008). This study applied an ischemic-hyperemic paradigm and a CASL scheme to study the flow heterogeneity between a variety of muscle groups (Wu et al. 2008). Another study used a clinical 3.0T scanner and standard coils in combination with the pulsed ASL technique FAIR-TrueFISP, to investigate perfusion response in the forearm musculature of healthy volunteers (Boss et al. 2006). While employing an intense exercise paradigm, good delineation could be achieved between active muscles and musculature not involved in the exercise technique. Using the same technique, it was feasible to assess perfusion changes in the relatively small Masseter muscle after sustained clenching (Schraml et al. 2011).

3.3.2 ASL in Peripheral Arterial Occlusive Disease

The first attempt to employ a continuous version of ASL to measure calf muscle perfusion in subjects with PAOD was realized using an ischemic-hyperemic paradigm to examine calf microvascular flow in 40 subjects with varying degrees of PAOD and 17 age-matched PAOD-free subjects. The authors applied a CASL scheme on a 3T scanner demonstrating that CASL flow measurements correlate with disease state as measured by ankle brachial pressure index and that those measurements exhibited preserved microvascular flow reserve in the presence of early to intermediate vascular disease (Wu et al. 2009).

A PASL method was used in another study to measure calf muscle perfusion in subjects with PAOD. The data of this study was acquired on a 3T scanner with a peak exercise paradigm to measure flow in 15 healthy volunteers and 15 age-matched patients with PAOD. In this study the Q2TIPS [QUIPSS (Quantitative Imaging of Perfusion Using a Single Subtraction) II with thin-slice TI1 periodic saturation] sequence was implemented. Q2TIPS minimizes errors caused by variable transit delay and deletes the intravascular signal (Pollak et al. 2012). In this study a higher peak exercise calf perfusion was found in healthy volunteers in comparison to PAOD patients, thus differentiating healthy from PAOD patients. Moreover, in the healthy subjects, the anterior tibialis and gastrocnemius revealed to be the calf muscles with the highest perfusion rate. In contrast for the PAOD group the calf muscle with the highest perfusion was the anterior tibialis muscle. The within subject correlation coefficient between repeated studies was 0.87 and the interobserver reproducibility was 0.96 indicating both reliability and reproducibility (Luh et al. 1999).

In conclusion ASL may prove useful for the evaluation of disease progression in PAOD. Those patients unable to receive contrast agents may profit from perfusion imaging with ASL. Clinical trials in a large patient collective are warranted to further elucidate the application of ASL in PAOD.

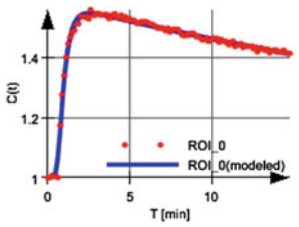

Fig. 14 Typical time-intensity curve derived from a subcutaneous tumor. The initial upslope describes the wash in phase and the subsequent downslope the washout phase. In DCE-MRI quantitative analysis the whole curve is used to calculate single values of different microvascular parameters

4 Part 3 Dynamic Contrast Enhanced (DCE)-MRI

4.1 General Principles of Dynamic Contrast Enhanced (DCE)-MRI

4.1.1 Origin of the DCE-MRI Signal and Technical Principles

Dynamic contrast enhancement (DCE) is the temporal study of the tissues response to an intravenously injected bolus of contrast agent (CA). This technique is conducted through acquisition of baseline native images, followed by a series of images acquired over time after administration of the CA.

A paramagnetic CA is present into the vascular system of a subject over a short period of time. The CA disperses and as it enters a tissue, it changes the MR signal intensity of the tissue to a degree that is associated with its local concentration. The induced signal intensity variation of the tissue is monitored over time through a serial acquisition of images every few seconds. This signal is used to plot a so-called time-intensity curve (TIC, Fig. 14) for the tissue which reflects the tissue's response to the arrival of the CA. Through the analysis of this curve, certain physiological properties that are related to the microvascular blood flow can be derived, such as vessel permeability, vessel surface area product and tissue volume fractions.

In a typical DCE-MRI imaging session, a region of interest (ROI) is selected and MR images are collected. Each image acquired corresponds to one time point, and each pixel in each set of images generates its own time course of intensity values. Images of the resultant changes in signal intensity can then be analyzed to derive parametric maps of specific microvascular biomarkers (Fig. 15). These parameters generally reflect the two-compartment pharmacokinetics exhibited by contrast agents, comprising of intravascular and extravascular components.

A paramagnetic particle will induce changes in the MRI-signal of a tissue, through which it passes due to two different physical–chemical properties:

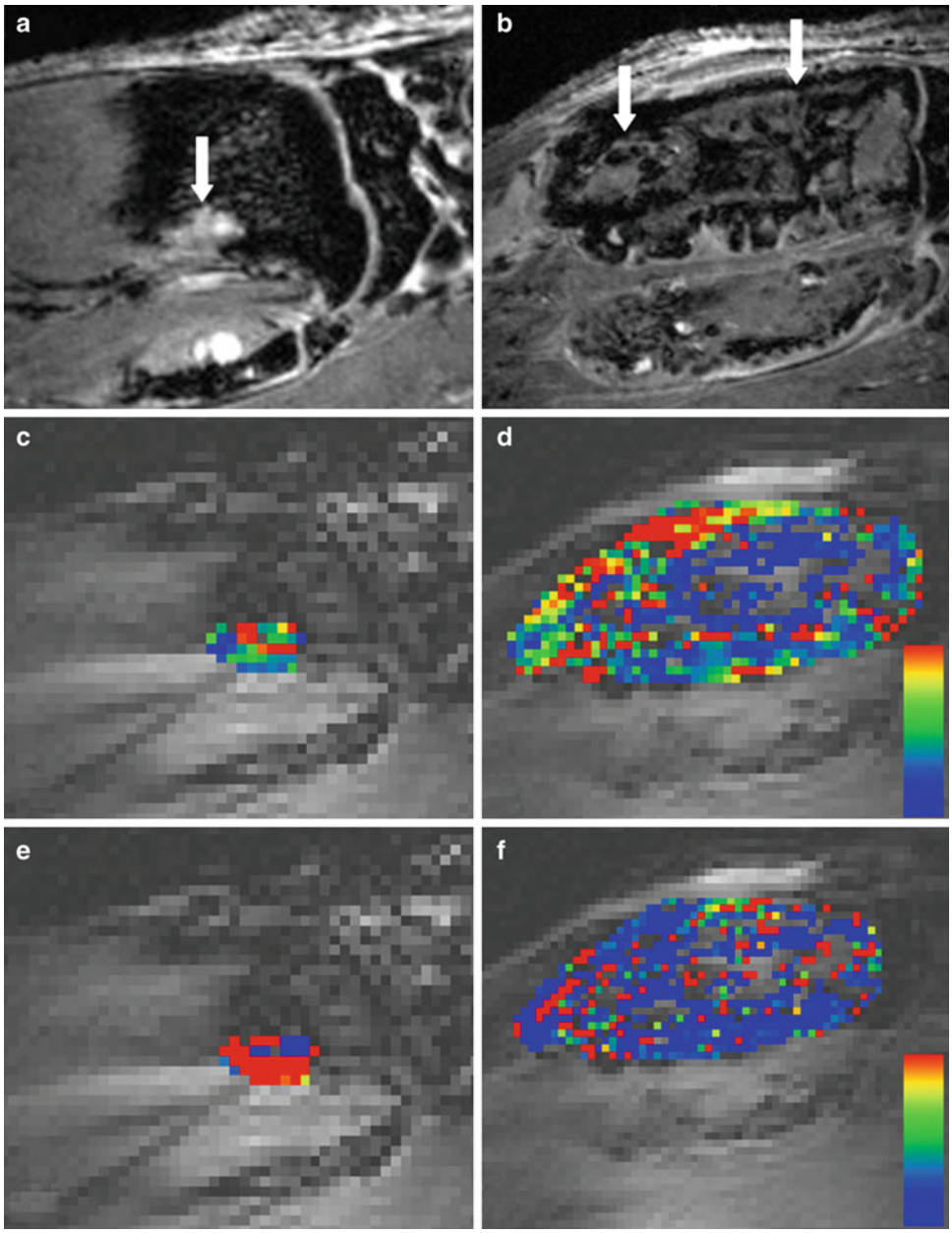

Fig. 15 Comparison of treated experimental breast cancer bone metastases-bearing rats at day 30 after tumor cell injection; *T*1-weighted MRI after contrast agent application (**a**), DCEMRI-derived color-coded maps for amplitude *A* (**c**), and exchange rate constant k_{ep} (**e**) with sham-treated rats; *T*1-weighted MRI after contrast agent application (**b**), DCEMRI-derived color-coded maps for amplitude *A* (**d**), and exchange rate constant k_{ep} (**f**). *Arrows point* to soft tissue parts of bone metastases. DCEMRI color code; *red color* indicates higher values and *blue color* depicts lower values for amplitude *A* (**d**) and exchange rate constant k_{ep} (*f*)

1. Reduction of tissue relaxation times *T*1 and *T*2 through diffusible CA (relaxation effect). This effect is used to generate positive enhanced *T*1 weighted images and the technique is called DCE-MRI or *T*1-W DCE or Dynamic Relaxivity MRI.
2. Transient formation of magnetic field heterogeneities during the passage of a paramagnetic CA through the capillaries (susceptibility effect). This effect is used to produce negative enhanced *T*2 or *T*2* weighted images. Studies assessing this effect are commonly referred to *dynamic susceptibility contrast* (DSC) MRI or *T*2-W DCE (Themen 1997).

4.1.2 Data Acquisition Using DCE-MRI

For data acquisition using DCE-MRI three steps are required:

(1) Recording a map of the native *T*1 values ($T1_0$ map) before contrast administration, as the calculation of the CA concentrations also requires knowledge of the initial *T*1 value of the tissues prior to CA arrival (Yankeelov and Gore 2009).

(2) Acquisition of heavily *T*1-weighted images before and after CA introduction. Quick acquisition of heavily *T*1-weighted images is commonly carried out by spoiled gradient echo sequences (synonym: fast low angle

shot = FLASH). Using a saturation-recovery-turbo FLASH sequence enables estimation of precontrast *T*1 relaxation times derived from the dynamic image series (Brix et al. 2004).

(3) The arterial input function (AIF) is a method to estimate the concentration of the CA in the blood plasma of a feeding vessel as a function of time.

Acquiring the AIF is essential for nearly all quantitative analysis methods. A perquisite of pharmacokinetic models is the arrival of the CA at the tissue in the form of an ultra-narrow, well-defined bolus (i.e., impulse input of tracer) (Themen 1997). This ideal bolus will flood the tissue and create a response, a concentration time curve within the tissue, which is termed the residue (or residual) response. It is this curve that can be used to extract quantitative information regarding intrinsic tissue properties. However, in reality the concentration time course of the CA in a vessel entering the tissue (the AIF) differs substantially from the ideal form and hence the residual function cannot be measured directly (Fig. 16). Alternatively concentration times curves of both the tissue and a feeding artery (AIF) can be measured whereupon these two curves can be used to reconstruct the residual function and quantification can performed accurately. The mathematical process of deriving information in order to reconstruct an underlying unknown original function (in our case the residual function) which has been altered by a second function (the AIF) to consequently produce a third function (tissue concentration time course) is termed deconvolution.

In practice the form of the CA bolus is affected by individual parameters, such as CA dose, injection technique, cardiovascular status, and other physiological variables. These variations can be minimized by the deconvolution of data from each voxel using the AIF. The analysis relies on the measurement of a surrogate AIF from a major feeding artery which equals only an approximation of the true AIF.

The number of measurements required for data acquisition is dependent on the quantification method one wishes to apply. For simple semiquantitative analysis of signal intensity curves, method 2 will suffice. For additional CA concentration values method 1 must also be included. For quantitative pharmacokinetic analysis all three methods should take place.

4.1.3 DCE Analysis Procedure

Shortly after a bolus of paramagnetic contrast agent is intravenously administered it enters the tissue. The enhancement pattern of the tissue depends on a wide variety of factors, including but not limited to vascularity, capillary permeability, perfused capillary surface area, volume and composition of extracellular fluid, renal clearance and tissue perfusion. The analysis of the contrast enhancement pattern can be performed using a variety of techniques, such as simple semiquantitative methods, analysis of curve morphology and quantitative methods. Simple semiquantitative values can be derived from the tissue time-intensity curve alone. More complex pharmacokinetic based analyses require the identification of the AIF.

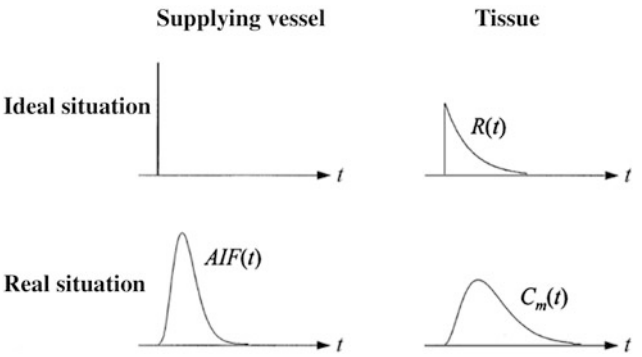

Fig. 16 Should a CA arrive at the tissue as an ideal, ultra-narrow flooding bolus, the tissue response is the sought after residual function. In reality the form of the bolus in the feeding artery (the AIF) differs substantially from the ideal form. The measured signal in the tissue is not the residual function but a widely spread time-concentration curve. From Themen (1997). This material is reproduced with permission of Springer

4.1.4 Semiquantitative Analysis

The signal intensity curve alone is very helpful for simple semiquantative analysis.

Model-free parameter extractions have several advantages as they are (1) robust, (2) obviate the need for an AIF measurement, (3) some of them, such as area under-curve (AUC) are independent of injection protocols (Galbraith et al. 2002), (4) easy to calculate, and (5) do not have any rigorous requirements in terms of data acquisition (Jaspers et al. 2010). Regrettably semiquantitative parameters do not necessarily have any obvious physiological correlates, since they represent a mix of microcirculatory and tissue properties. The degree to which each of these physiological parameters contributes is challenging to determine. Another limitation is the fact that most of the signal intensity based methods are influenced by the type of acquisition protocol applied. They depend on factors such as sequence parameters, hardware settings, scan duration, amount of administered CA (Lavini et al. 2007), CA properties, injection protocol and so on. These varations will occur even if identical sequences are used since the baseline signal for any given tissue, using a particular sequence, will differ by the choice of imager. In summary the comparison

of semiquantitative studies are difficult and should be made with caution due to the aforementioned variations.

Having said this, semiquantitative parameters reflect physiological mechanisms and qualitative signal based analysis is very useful, especially where measurement of relative changes in an individual or group of patients is required.

Commonly used metrics for this measurement technique include:

1. *Initial area under the curve (iAUC)*: computes the area under tissue concentration time curve up to a stipulated time that includes a major portion of tissue response.
2. *Maximum (relative) enhancement* (in %): maximum signal difference (MSD)/signal baseline (SB).
3. *Time to maximum signal intensity* (in sec.): time between the arterial peak enhancement and SI_{max}.
4. *Time to peak enhancement* (in sec.): time between the arterial peak enhancement and the end of the steepest portion of enhancement.
5. *Rate of peak enhancement*: [(SIend − SIprior/(SIbase × T)] × 100 (in %/min).
6. *Rate of enhancement*: [(SImax – Slbase)/(SIbsae × Tmax)] × 100 (in %/min).

The slope of the time-intensity curve can also be normalized by dividing it with the arterial TIC slope. This parameter is termed perfusion index (PI) by some authors and has been used both in studies of skeletal muscle and the myocardium (Isbell et al. 2007; Jiji et al. 2013; Panting et al. 2002).

7. *T90* (in sec.): Measurement of the time taken for the tissue to attain 90 % of its subsequent maximal enhancement.
8. *Maximum rate of change of enhancement* (maximal intensity change per time interval ratio)(in %/min).

The last two parameters are designed to minimize the variation which occurs between patients as a result of variations in contrast dose, injection, scanning techniques, and scanner type (Jackson 2004).

Semiquantitative analysis can also be applied performing *first-pass methods*. These methods are easily implemented in clinical settings with relatively low scanning time. It is assumed that the dynamic enhancement pattern observed early during the first pass (the slope) will represent above all, the kinetics of the contrast agent within the blood vessels. The method has been applied in several studies of cervical cancer (Mayr et al. 1996, 2000) and other variations of the method have been applied extensively in studies of the heart (Panting et al. 2002; Pack and DiBella 2010; Saeed 2001) and the skeletal muscle (see section Investigations of the musculoskeletal system with DCE-MRI techniques).

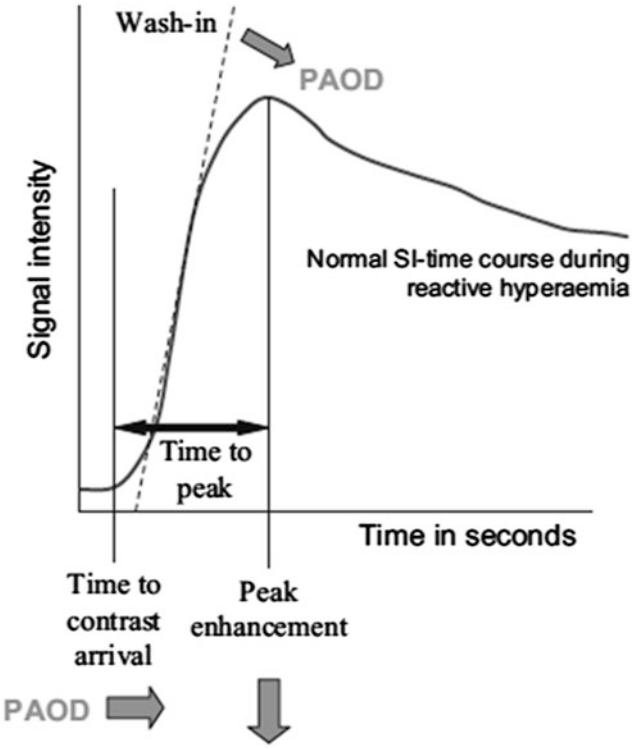

Fig. 17 Diagram of a signal intensity curve of DCE-MRI, representing the contrast agent dependent signal intensity over time. Characteristic curve segments are the linear upslope (wash-in) reaching a maximum intensity, i.e., peak enhancement. Subsequently, there is a washout of contrast medium. The time to peak describes the time from onset of bolus appearance (time to contrast arrival) to peak contrast enhancement. The perfusion reserve of patients can be assessed by measuring the reactive hyperemia after occluding the arterial inflow by suprasystolic cuff compression or after symptom-limited treadmill exercise in comparison with age-matched controls. In case of peripheral arterial occlusive disease (PAOD), there is a delay in contrast arrival time, a less steep upslope, and a lower peak enhancement (*arrows*). From Weber et al. (2007). This material is reproduced with permission of Springer

4.1.5 Morphologic Analysis

This approach primarily considers the shape of the uptake and washout of the TIC and has been named "curve-ology" (Yankeelov and Gore 2009). Distinctive curve patterns are defined and attempts are made to assign them to physiological or pathological findings (Van Rijswijk et al. 2001). For instance in the skeletal muscle, a rapid signal intensity increase followed by a narrow peak and a washout phase is evident for an adequate vascular reserve. In contrary, should the signal intensity curve shows a shallow increment, a delayed peak and only a weak or absent washout after exercise, this might be a hint toward a limited vascular reserve (Leppek et al. 2004) (Fig. 17). The method has been successfully applied to rheumatoid arthritis (Van de Sande et al. 2012; Van der Leij et al. 2009), breast imaging (Rieber

et al. 2002) and a variety of musculoskeletal lesions (Lavini et al. 2007).

4.1.6 DCE Quantitative Analysis

One of the appealing features of DCE-MRI is its capability to calculate absolute measures directly related to the physiological and pathophysiological properties of the microvascular environment and the surrounding tissue. This is usually performed by means of model-based pharmacokinetic analysis. The purpose of a model is to describe the underlying physiological phenomenon in mathematical terms in order to enable the estimation of specific tissue parameters from a measured signal. Tracer kinetic models describe tracer transport processes within the tissue. The model should adequately describe the aspects relevant for the investigation. To this end the result of a quantitative analysis is model dependent.

The fundamental physiological parameters describing the CA movement across the vascular endothelium include: vessel wall permeability, vessel surface area, intravascular and extracellular extravascular volume fractions, blood flow (i.e., perfusion) and ratios of the CA concentrations across the endothelium.

With model-based quantitative analysis three relevant microscopic parameters for the characterization of the microcirculation are acquired: CA exchange rates between the capillaries and the interstitial tissue (the so-called capillary permeability), regional blood volumes, and regional blood flow.

To enable quantitative analysis the following steps are performed:

a. Measurement of baseline $T1$ before gadolinium injection (this enables transformation of the signal intensity-time curve into a time-concentration curve).
b. Measurement of signal intensity changes before and after CA application in the tissue.
c. Conversion of signal intensity data to CA concentrations: The conversion of signal intensity curves into time-concentration curves is carried out by means of an appropriate signal-model since in MRI there is no direct correlation between CA concentration and measured signal intensity changes.
d. Computed time-concentration curves (TCC) are analyzed by tracer kinetic modeling using curve-fitting techniques, either on a region of interest or, less commonly, on a pixel-by-pixel basis.

4.1.7 Curve Fitting

The bulk of quantitative analyses techniques rely on curve-fitting methods to produce estimates of parametric values. Each model is an equation containing multiple numbers of free fitting (adjustable) parameters. These are the physiological parameters which are extracted in order to ascertain receipt of significant information about the tissue. By varying the parameters' values in those equations using mathematical algorithms (for example nonlinear least squares fit), a parameter combination that best fits the observed TCC is sought. Pharmacokinetic analysis and interpretation of dynamic data are complex and computationally demanding. It is complicated by the availability of a plethora of analysis algorithms and by the fact that some calculated parameters may represent different biological phenomena depending on the model applied. Model derived pharmacokinetic parameters have the advantage of being more directly related to physiological events in the tissues and are potentially independent of the type of scanner, scanning technique, or individual patient variations. Longitudinal studies as well as accurate comparison between results are very well doable.

4.2 Dynamic Susceptibility MRI

In conventional MRI local magnetic heterogeneities arise on the boundaries between structures that differ in their magnetic susceptibility leading to signal reduction on $T2^*$ weighted gradient echo sequences (Themen 1997) (Fig. 18). The same effect occurs when a paramagnetic CA resides in the intravascular space of a tissue. Thus, this effect can only be utilized in tissues where specific vascular barriers prevent a fast passage of the CA into the interstitial space such as brain, retina, and testes. Alternatively, the use of intravascular (blood pool) contrast agents, which leave the vessels at a much slower rate, are warranted.

In DSC a CA bolus is quickly injected intravenously and the resulting transient $T2^*$ reductions are monitored during the first passage of the CA through the capillary bed. The rapid loss of MR signal on $T2^*$ weighted images is measured and then used to calculate the change in concentration of CA for each individual voxel. The conversion of time-intensity curves into time-concentration curves is utilized to calculate estimates of local blood volume and flow. The transient signal reduction is proportional to local blood volume and flow (Fig. 19).

4.2.1 Data Acquisition Using DSC MRI

The typical imaging technique for DSC is single or multi-shot echo-planar imaging (EPI).

Either spin echo or gradient echo sequences can be employed. Spin echo sequences minimize the signal contribution from large vessels, gradient echo sequences maximize $T2^*$ weighting (Essig et al. 2002).

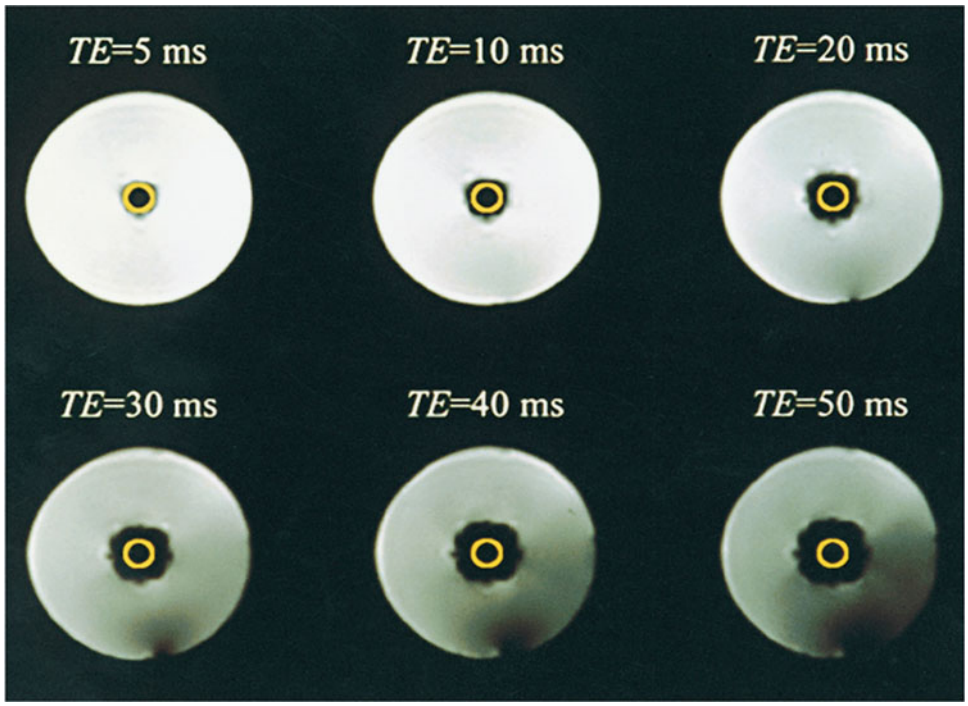

Fig. 18 $T2^*$-W images of a tube filled with a Gd-DTPA solution within a water phantom. The signal reduction effect increases as the echo times are prolonged (i.e., the stronger the $T2^*$-W). From Themen (1997). This material is reproduced with permission of Springer

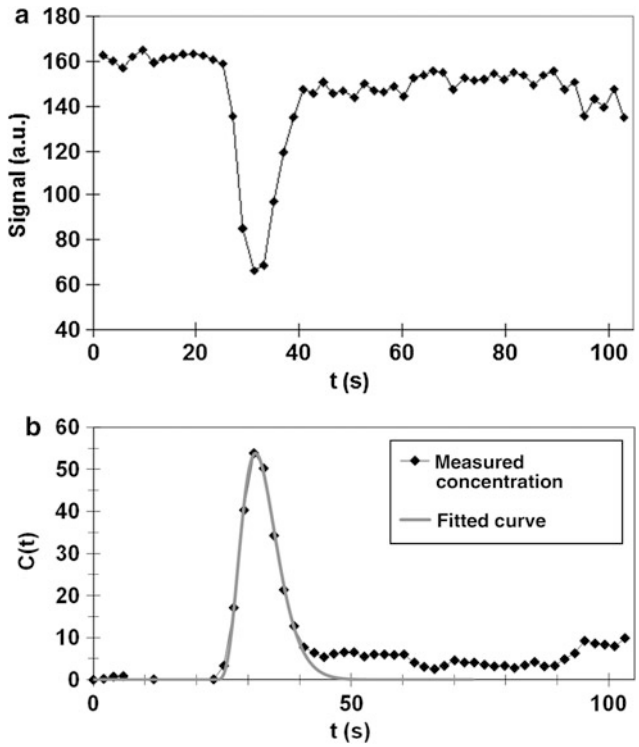

Fig. 19 Conversion of a signal time-intensity curve (**a**) into a time-concentration curve (**b**). The signal time-intensity curve (**a**) depicts the signal loss during the passage of a CA through a tissue, which is registered with a $T2^*$-weighted GE-EPI sequence. The relative blood volume is proportional to area under the time-concentration curve (**b**). From Weber et al. (2005). This material is reproduced with permission of Springer

4.2.2 DSC Quantification Approaches

The main objectives of DSC MRI are the measurement of:

(a) *Regional blood volume* (rBV): volume (ml) of blood perfused vessel in a voxel divided by the tissue mass in the voxel (g).

(b) *Mean transit time* (MTT): average transit time of a tracer particle through the capillary bed.

(c) *Regional blood flow* (rBF): i.e., perfusion (milliliters per minute).

Analysis of DSC MRI data works with the assumption that the contrast agent remains within the vascular space throughout the examination acting as an intravascular CA (blood pool). As mentioned earlier this assumption is only valid for very few tissues and naturally not for tumors. Therefore, the application of DCS was initially limited to studies of normal brain although modifications of the technique have subsequently allowed its use in other tissues.

The standard approach for estimating absolute blood flow from the obtained data includes four steps:

1. The time-concentration data from an individual voxel are deconvolved with an arterial input function (AIF), derived from a major vessel (O'Connor et al 2011).
2. The area under the contrast concentration curve is used for an analytical calculation to estimate the blood volume (BV) within the pixel.
3. The mean transit time (MTT) is then estimated using some form of a standardized relationship between the surface and the height of the time-concentration curve.
4. Blood flow is calculated using the central volume theorem: $rBF = rBV/MTT$ ($ml \cdot min^{-1} \cdot g^{-1}$).

Challenges exist, which makes the estimation of absolute flow complex (O'Connor et al 2011). Quantitative measurements are complicated by the following factors: Contrast leakage and subsequent tissue enhancement, contrast recirculation, bolus dispersion and accurate estimation of rBV and MTT.

The most prevailing clinical applications of DSC are stroke (Wang et al. 2012; MacDonald et al. 2011), cerebrovascular insufficiency (Crane et al. 2012; Calviere et al. 2012) and brain tumors (Aronen et al. 1993, 1994), though it has been used on occasion to measure muscle perfusion in animal experiments (Rissanen et al. 2005; Goyault et al. 2012).

4.2.3 DCE and DSC MRI Combination Approaches

Dual-echo DSC MRI can be used to simultaneously extract reliable DCE-MRI kinetic parameters (related to extravasation) in addition to conventional blood volume and blood flow metrics. The feasibility of separately measuring $T1$- and $T2^*$-weighted induced signal changes using dual-echo pulse sequences was conducted in studies of brain tumors (Kuperman et al 1996; Vonken et al. 2000; Barbier et al. 1999). When combined with a precontrast $T1$ map the dual-echo DSC MRI technique enables reliable determination of K^{trans} and v_e. These parameters showed a high degree of correlation with the DSC MRI-derived measurements (Quarles et al. 2012) (Table 1).

4.3 Investigations of the Musculoskeletal System with DCE-MRI Techniques

4.3.1 Human Studies

Early DCE-MRI studies of the muscle focused on assessing the potential of the technique for distinguishing between malignant and benign conditions using semiquantitative slope values. Though significant differences were found between benign compared to malignant tissues and the method exhibited fair sensitivity, a significant overlap persisted between malignant neoplasms and several highly vascularized benign lesions (Verstraete et al. 1994; Konez et al 1997; Van der Woude et al. 1998). A variety of musculoskeletal (MSK) pathological conditions have been investigated with the previously described semiquantitative curve shape analysis method (Lavini et al. 2007). Although the shape maps obtained revealed a significant heterogeneity of TIC patterns within the lesions, the method was not able to differentiate malignant from benign. In patients suffering from medial tibial pain the sensitivity of DCE-MRIs to depict periosteal edema was compared to other MRI sequences such as proton density, $T2$ weighted and post-contrast $T1$ weighted images (Mattila et al. 1999). The gradually enhancing periostitis was best demonstrated by DCE-MRI in comparison to the other techniques.

Similar to other functional MRI methods, DCE uses the hyperemia and exercise paradigms to investigate muscle perfusion. The majority of perfusion experiments using the technique were directly performed on patients with PAOD (discussed in the section below). DCE measurements of the calf of four healthy young adults performing a plantar flexion exercise paradigm at different workloads were compared with blood flow in the popliteal artery by ultrasonography. The collected MRI parameters enabled to visually separate the muscles into an exercising and non-exercising group. However, the increase in SI measured by MRI was much smaller compared to the increase in blood flow values acquired from ultrasonography and the correlation between the two measurements was limited (Nygren et al. 2000).

A further investigation applied a postarterial occlusion paradigm leading to reactive hyperemia for assessing the first pass perfusion in the calf muscle of 20 healthy volunteers. Applying the general Tofts model (Tofts et al. 1999) for quantification, the data was then compared to corresponding measurements from segmental volume plethysmography. Results showed highly significant changes in calf muscle signal dynamics in the hyperemic leg versus those in the contralateral resting leg, both when applying semiquantitative and deconvolution (quantitative) analysis. Furthermore, flow extraction fraction products within the non-compressed leg were in agreement with published resting perfusion values (Lutz et al. 2004).

In 2005 a new method was described to quantitatively measure skeletal muscle first pass blood flow during post-ischemic reactive hyperemia without the requirement of deconvolution. This method uses the quick release of an occlusive thigh cuff to deliver a step-input of CA that was injected after cuff inflation. The simple input function required only the optimization of Larsson's model (Larsson et al. 1994) to extract K^{trans} (or $K_i = E{\cdot}F$) and v_e. The authors compared the DCE protocol to blood flow studies with the same volunteers, using phase-contrast velocimetry (PCV) obtained from the popliteal artery. The results for the distribution volume (v_e) were in good agreement with values reported in the literature and correlated significantly with the blood flow studies with the same volunteers, though the PCV yielded significantly lower flow values. DCE blood flow values were significantly different in the observed muscle groups and correlated well with the known distribution of different muscle fibers (Thompson et al. 2005).

4.3.2 Animal Studies

Similar to human studies the majority of animal experiments examining muscle microperfusion deal with PAOD.

Table 1

Symbol	Name	Definition	Units
K^{trans}	Transfer constant (or coefficient)	Volume transfer constant between blood plasma and EES	min^{-1}
k_{ep}	Rate constant[a]	Rate constant between EES and blood plasma (backflux exchange rate)	min^{-1}
v_e	Volume of extravascular extracellular space (EES)	Volume of extravascular extracellular space per unit volume of tissue	None (values either $0 < v_e < 1$ or as %)

[a] $K_{ep} = K^{trans} / v_e$

Table 2

Quantity	Definition	Unit
C_a	Tracer concentration in arterial whole blood	mM = 1 mmol/L
C_e	Tracer concentration in EES	mM
C_p	Tracer concentration in arterial blood plasma	mM
C_t	Tracer concentration in tissue	mM
C_v	Tracer concentration in venous whole blood	mM
CL_d	Distribution clearance	ml min^{-1}
E	Initial extraction ratio (fractional reduction in capillary blood concentration of a CA as it passes through tissue)	None (%)
Hct	Hematocrit	None
F	Perfusion (or flow) of whole blood per unit mass of tissue	ml g^{-1} min^{-1}
P	Total permeability of capillary wall	cm min^{-1}
PS	Permeability surface area product per unit mass of tissue	ml min^{-1} g^{-1}
S	Surface area per unit mass of tissue	cm^2 g^{-1}
V_b	Total whole blood volume[a]	ml
V_e	Total EES volume[a]	ml
V_p	Total blood plasma volume[a]	ml
V_t	Total tissue volume[a]	ml
v_b	Whole blood volume per unit volume of tissue[a]	None (%)
v_p	Blood plasma volume per unit volume of tissue	None (%)
λ	Tissue blood partition coefficient	ml g^{-1}
ρ	Density of tissue	g ml^{-1}

[a] $V_b = v_b V_t$; $V_e = v_e Vt$; $V_p = v_p V_t = (1 - Hct) V_b$
C = concentrations (mM)
V = total volumes (ml)
v = fractional volumes (%)
e, a, p, t, v = extravascular extracellular space, arterial blood, plasma, tissue, venous respectively [for example: k_{ep} stands for—constant (k) extravascular extracellular space ($_e$) to plasma ($_p$)]

Mainly utilizing the well-established arterial ligation model (Jaspers et al. 2010; Rissanen et al. 2005; Luo et al. 2002; De Lussanet et al. 2007; Ziv et al. 2004) several experiments have successfully quantified muscle perfusion in small animals using both DCE-MRI (Luo et al. 2002; De Lussanet et al. 2007; Ziv et al. 2004; Loerakker et al. 2011; Faranesh et al. 2006; Cheng 2007) and DSC MRI (Rissanen et al. 2005; Goyault et al. 2012) administering a variety CAs [including blood pool agents (Jaspers et al. 2010; Ziv et al. 2004; Faranesh et al. 2006; Cheng 2007) and Superparamagnetic Iron Oxide Particles (Rissanen et al. 2005)].

4.3.3 Peripheral Arterial Occlusive Disease

Blood flow to the lower leg muscles were quantified at rest and after individually adjusted plantar flexion muscular exercise in five subjects: A female patient with PAOD (Fontaine IIb) before and after PTA, a male patient with coronary heart disease without clinical signs of a PAOD, a

healthy volunteer and two professional athletes. The semi-quantitative analysis showed distinctive exercise induced changes of the upslope, wash-in, peak and washout of the SI-curves in the different muscles of the calf in all subjects. The magnitude of the changes induced also seemed to be dependent on the individual fitness of the subjects. Notably, the PAOD patient demonstrated a steeper SI-curve post-exercise after PTA (Leppek et al. 2004).

A sequence was presented enabling simultaneous acquisition of the arterial input function and tissue perfusion images. The technique utilized a saturation recovery GRE sequence for the estimation of the AIF, interleaved with an inversion-recovery GRE sequence for the measurement of tissue perfusion. Though the study did not employ model based analysis, a normalized perfusion index (PI) was defined as the slope of the time-intensity curve in muscle divided by the arterial TIC slope. First pass imaging was applied to the measurement of the PI in 11 patients with mild to moderate symptomatic PAOD and 22 normal subjects directly after peak exercise. In the PAOD group the ankle-brachial index (ABI) failed to correlate with PI. Neither the ABI nor the PI correlated with the workloads achieved (PAOD patients approx. 450 J, normal subjects approx. 1,100 J). Interestingly, peak-exercise measurements were able to distinguish PAOD patients from normal subjects (Isbell et al. 2007).

New methods were applied to determine the utility and reproducibility of rest, exercise, and perfusion reserve (PR = ratio of exercise to rest blood flow) measured by DCE-MRI. Tissue perfusion and arterial input both at rest and peak exercise in the calves of PAOD patients with claudication and age-matched controls were investigated. Though highly reproducible, rest perfusion parameters were too variable and too low in the muscle to distinguish between controls and PAOD patients. This held also true for the PR which was reproducible but highly variable as well. The exercise parameters could distinguish between patients and healthy volunteers (Jiji et al. 2013).

Recently, the ability of DCE to reproducibly asses the functional peripheral vascular status was tested. In this study the first pass step-input method was used (Thompson et al. 2005) extracting the influx constant K_i ($K^{\text{trans}} = E{\cdot}F{\cdot}_p (1 - Hct)$ and K_i is defined as $E{\cdot}F$). Besides, the area under the curve up to 90 s after CA arrival was calculated. Inter-scan and inter-reader reproducibility were determined as well. The reproducibility of DCE-MRI to measure microvascular function was poor in patients due to large inter-scanvariations (Versluis et al. 2011). In a similar study Gadofosveset, a blood pool CA (Blood pool agents are a CA group, also referred to as intravascular CA, which in contrast to conventional contrast agents leave the intravascular space at a much slower rate) was used. The pharmacokinetic parameters v_p and k were significantly lower for all muscle groups in PAOD patients as compared to healthy control subjects (Versluis et al. 2012) (Table 2).

DCE-MRI has been applied for studying plaque neovascularization in animals and patients with atherosclerosis (Kerwin et al. 2003; Calcagno et al. 2008). Plaque angiogenesis is an attractive target to identify asymptomatic yet high-risk atherosclerotic lesions.

5 Conclusion

Muscle BOLD MRI has proven to be a very sensitive tool to detect microvascular pathologies in a variety of different disease settings. Despite its multifactorial origin in skeletal muscle tissue, the BOLD contrast primarily depends on perfusion related changes of muscle tissue oxygenation. However, current muscle BOLD studies often suffer from the uncertainty of uncontrolled parameters influencing the $T2^*$ signal. ASL allows a direct measurement of microvascular perfusion and—as BOLD MRI—is independent of the administration of contrast agents but suffers from a bad signal to noise ratio and the need of additional parameter measurements or assumptions what may compromise the resulting datasets. With DCE, microvascular properties, such as fractional volumes of plasma and blood, vessel permeability and perfusion can be obtained. If these MR techniques are to find their way into the clinics, standardization, further validation, and reproducibility experiments must precede.

References

Alsop DC, Detre JA (1996) Reduced transit-time sensitivity in noninvasive magnetic resonance imaging of human cerebral blood flow. J Cereb Blood Flow Metab 16:1236–1249

Alsop DC, Detre JA (1998) Multisection cerebral blood flow MR imaging with continuous arterial spin labeling. Radiology 208:410–416

Alsop DC, Detre JA, Grossman M (2000) Assessment of cerebral blood flow in Alzheimer's disease by spin-labeled magnetic resonance imaging. Ann Neurol 47:93–100

Amarteifio E et al (2011) Dynamic contrast-enhanced ultrasound for assessment of skeletal muscle microcirculation in peripheral arterial disease. Invest Radiol 46:504–508

Amarteifio E et al (2013) Assessment of skeletal muscle microcirculation in type 2 diabetes mellitus using dynamic contrast-enhanced ultrasound: a pilot study. Diab Vasc Dis Res. doi:10.1177/1479164113484165 (Epub ahead of print)

Aronen HJ, Cohen MS, Belliveau JW, Fordham JA, Rosen BR (1993) Ultrafast imaging of brain tumors. Top Magn Reson Imaging 5:14–24

Aronen HJ et al (1994) Cerebral blood volume maps of gliomas: comparison with tumor grade and histologic findings. Radiology 191:41–51

Baligand C et al (2011) Measuring perfusion and bioenergetics simultaneously in mouse skeletal muscle: a multiparametric functional-NMR approach. NMR Biomed 24:281–290

Bandettini PA, Wong EC, Hinks RS, Tikofsky RS, Hyde JS (1992) Time course EPI of human brain function during task activation. Magn Reson Med 25:390–397

Barbier EL et al (1999) A model of the dual effect of gadopentetate dimeglumine on dynamic brain MR images. J Magn Reson Imaging 10:242–253

Berglund B, Eklund B (1981) Reproducibility of treadmill exercise in patients with intermittent claudication. Clin Physiol (Oxford England) 1:253–256

Bertoldi D et al (2006) New insight into abnormal muscle vasodilatory responses in aged hypertensive rats by in vivo nuclear magnetic resonance imaging of perfusion. J Vasc Res 43:149–156

Blamire AM, Styles P (2000) Spin echo entrapped perfusion image (SEEPAGE). A nonsubtraction method for direct imaging of perfusion. Magn Reson Med 43:701–704

Boss A, Martirosian P, Claussen CD, Schick F (2006) Quantitative ASL muscle perfusion imaging using a FAIR-TrueFISP technique at 3.0 T. NMR Biomed 19:125–132

Boushel R et al (2000) Blood flow and oxygenation in peritendinous tissue and calf muscle during dynamic exercise in humans. J Physiol 524(Pt 1):305–313

Brix G et al (2004) Microcirculation and microvasculature in breast tumors: pharmacokinetic analysis of dynamic MR image series. Magn Reson Med 52:420–429

Bulte DP, Alfonsi J, Bells S, Noseworthy MD (2006) Vasomodulation of skeletal muscle BOLD signal. J Magn Reson Imaging 24:886–890

Bunt TJ, Holloway GA (1996) TcPO2 as an accurate predictor of therapy in limb salvage. Ann Vasc Surg 10:224–227

Buxton RB et al (1998) A general kinetic model for quantitative perfusion imaging with arterial spin labeling. Magn Reson Med 40:383–396

Calcagno C et al (2008) Detection of neovessels in atherosclerotic plaques of rabbits using dynamic contrast enhanced MRI and 18F-FDG PET. Arterioscler Thromb Vasc Biol 28:1311–1317

Calviere L et al (2012) Executive dysfunction in adults with moyamoya disease is associated with increased diffusion in frontal white matter. J Neurol Neurosurg Psychiatry 83:591–593

Carlier PG, Bertoldi D, Baligand C, Wary C, Fromes Y (2006) Muscle blood flow and oxygenation measured by NMR imaging and spectroscopy. NMR Biomed 19:954–967

Chalela JA et al (2000) Magnetic resonance perfusion imaging in acute ischemic stroke using continuous arterial spin labeling. Stroke 31:680–687

Cheng H-LM (2007) T1 measurement of flowing blood and arterial input function determination for quantitative 3D T1-weighted DCE-MRI. J Magn Reson Imaging 25:1073–1078

Crane DE et al (2012) Evaluating quantitative approaches to dynamic susceptibility contrast MRI among carotid endarterectomy patients. J Magn Reson Imaging 37:936–943

Dawson JM, Hudlicka O (1990) Changes in the microcirculation in slow and fast skeletal muscles with long term limitations of blood supply. Cardiovasc Res 24:390–395

De Lussanet QG et al (2007) Dynamic contrast-enhanced MRI of muscle perfusion combined with MR angiography of collateral artery growth in a femoral artery ligation model. NMR Biomed 20:717–725

Detre JA, Alsop DC (1999) Perfusion fMRI with arterial spin labeling. In: Bandettini PA, Moonen C (eds) Functional MRI. Springer, Berlin pp 47–62

Detre JA, Leigh JS, Williams DS, Koretsky AP (1992) Perfusion imaging. Magn Reson Med 23:37–45

Detre JA et al (1999) Noninvasive magnetic resonance imaging evaluation of cerebral blood flow with acetazolamide challenge in patients with cerebrovascular stenosis. J Magn Reson Imaging 10:870–875

Donahue KM, Van Kylen J, Guven S, Luh WM, El-Bershawi A, Bandettini PA, Hyde JS, Kissebah AH, Cox RW (1998) Simultaneous gradient-echo/spin-echo EPI of graded ischemia in human skeletal muscle. J Magn Reson Imaging 8:1106–1113

Duteil S et al (2004) Metabolic and vascular support for the role of myoglobin in humans: a multiparametric NMR study. Am J Physiol Regul Integr Comp Physiol 287:R1441–R1449

Duteil S et al (2006) Influence of vascular filling and perfusion on BOLD contrast during reactive hyperemia in human skeletal muscle. Magn Reson Med 55:450–454

Duyn JH, Tan CX, van Gelderen P, Yongbi MN (2001) High-sensitivity single-shot perfusion-weighted fMRI. Magn Reson Med 46:88–94

Essig M et al (2002) Dynamic susceptibility contrast-enhanced echo-planar imaging of cerebral gliomas. Effect of contrast medium extravasation. Acta Radiol 43:354–359

Fagrell B (1986) Microcirculatory methods for the clinical assessment of hypertension, hypotension, and ischemia. Ann Biomed Eng 14:163–173

Faranesh AZ, Kraitchman DL, McVeigh ER (2006) Measurement of kinetic parameters in skeletal muscle by magnetic resonance imaging with an intravascular agent. Magn Reson Med 55:1114–1123

Fox PT, Raichle ME (1986) Focal physiological uncoupling of cerebral blood flow and oxidative metabolism during somatosensory stimulation in human subjects. Proc Natl Acad Sci USA 83:1140–1144

Frank LR, Wong EC, Haseler LJ, Buxton RB (1999) Dynamic imaging of perfusion in human skeletal muscle during exercise with arterial spin labeling. Magn Reson Med 42:258–267

Frouin F et al (2006) An automated image-processing strategy to analyze dynamic arterial spin labeling perfusion studies. Application to human skeletal muscle under stress. Magn Reson Imaging 24:941–951

Gabrielli A, Avvedimento EV, Krieg T (2009) Mechanisms of disease. Scleroderma. N Engl J Med 19:1989–2003

Galbraith SM et al (2002) Reproducibility of dynamic contrast-enhanced MRI in human muscle and tumours: comparison of quantitative and semi-quantitative analysis. NMR Biomed 15:132–142

Garcia DM, Duhamel G, Alsop DC (2005) Efficiency of inversion pulses for background suppressed arterial spin labeling. Magn Reson Med 54:366–372

Gati JS, Menon RS, Ugurbil K, Rutt BK (1997) Experimental determination of the BOLD field strength dependence in vessels and tissue. Magn Reson Med 38:296–302

Gerontol J et al (2009) Multiparametric NMR-based assessment of skeletal muscle perfusion and metabolism during exercise in elderly persons : preliminary findings. J Gerontol A Biol Sci Med Sci 64:968–974

Goyault G et al (2012) Diffusion-weighted MRI, dynamic susceptibility contrast MRI and ultrasound perfusion quantification of denervated muscle in rabbits. Skeletal Radiol 41:33–40

Green DJ, Spence A, Halliwill JR, Cable NT, Thijssen DHJ (2011) Exercise and vascular adaptation in asymptomatic humans. Exp Physiol 96:57–70

Green HJ et al (2012) Can increases in capillarization explain the early adaptations in metabolic regulation in human muscle to short-term training? Can J Physiol Pharmacol 90:557–566

Gu P, Xu A (2013) Interplay between adipose tissue and blood vessels in obesity and vascular dysfunction. Rev Endoc Metab Disord. doi: 10.1007/s11154-012-9230-8

Hennig J, Schreiber A, Scheffler K (2000) Time resolved observation of BOLD effect in muscle during isometric exercise. Proc Int Soc Magn Reson Med 8:122

Hickey NC, Hudlicka O, Simms MH (1992) Claudication induces systemic capillary endothelial swelling. Eur J Vasc Surg 6:36–40

Howseman AM, Bowtell RW (1999) Functional magnetic resonance imaging: imaging techniques and contrast mechanisms. Philos Trans R Soc Lond B Biol Sci 354:1179–1194

Huegli RW et al (2009) Effects of percutaneous transluminal angioplasty on muscle BOLD-MRI in patients with peripheral arterial occlusive disease: preliminary results. Eur Radiol 19:509–515

Isbell DC et al (2007) Calf muscle perfusion at peak exercise in peripheral arterial disease: measurement by first-pass contrast-enhanced magnetic resonance imaging. J Magn Reson Imaging 25:1013–1020

Jackson A (2004) Analysis of dynamic contrast enhanced MRI. Br J Radiol 77:S154–S166

Jacobi B et al (2012) Skeletal muscle BOLD MRI: from underlying physiological concepts to its usefulness in clinical conditions. J Magn Reson Imaging 35:1253–1265

Jacobi B et al (2013) Alterations of skeletal muscle microcirculation detected by blood oxygenation level-dependent MRI in a patient with granulomatosis with polyangiitis. Rheumatology (Oxford, England) 52, 579–581

Jaspers K et al (2010) Optimized pharmacokinetic modeling for the detection of perfusion differences in skeletal muscle with DCE-MRI: effect of contrast agent size. Med Phys 37:5746

Jiji RS et al (2013) Reproducibility of rest and exercise stress contrast-enhanced calf perfusion magnetic resonance imaging in peripheral arterial disease. J Cardiovasc Magn Reson 15:14

Katoh M, Spuentrup E, Barmet C, Stuber M (2008) Local re-inversion coronary MR angiography: arterial spin-labeling without the need for subtraction. J Magn Reson Imaging 27:913–917

Kerwin W et al (2003) Quantitative magnetic resonance imaging analysis of neovasculature volume in carotid atherosclerotic plaque. Circulation 107:851–856

Kim SG (1995) Quantification of relative cerebral blood flow change by flow-sensitive alternating inversion recovery (FAIR) technique: application to functional mapping. Magn Reson Med 34:293–301

Konez O et al (1997) Gradient-echo perfusion imaging of musculoskeletal abnormalities with contrast-enhanced two-dimensional fat-saturation FLASH. J Magn Reson Imaging 7:895–902

Kober F et al (2004) High-resolution myocardial perfusion mapping in small animals in vivo by spin-labeling gradient-echo imaging. Magn Reson Med 51:62–67

Kos S et al (2009) Simultaneous dynamic blood oxygen level-dependent magnetic resonance imaging of foot and calf muscles: aging effects at ischemia and postocclusive hyperemia in healthy volunteers. Invest Radiol 44:741–747

Krix M et al (2011) Comparison of transient arterial occlusion and muscle exercise provocation for assessment of perfusion reserve in skeletal muscle with real-time contrast-enhanced ultrasound. Eur J Radiol 78:419–424

Kuperman VY et al (1996) Differentiating between T1 and $T2^*$ changes caused by gadopentetate dimeglumine in the kidney by using a double-echo dynamic MR imaging sequence. J Magn Reson Imaging 6:764–768

Kwong KK et al (1992) Dynamic magnetic resonance imaging of human brain activity during primary sensory stimulation. Proc Natl Acad Sci USA 89:5675–5679

Kwong KK et al (1995) MR perfusion studies with T1-weighted echo planar imaging. Magn Reson Med 34:878–887

Larsson HB, Stubgaard M, Søndergaard L, Henriksen O (1994) In vivo quantification of the unidirectional influx constant for Gd-DTPA diffusion across the myocardial capillaries with MR imaging. J Magn Reson Imaging 4:433–440

Lavini C et al (2007) Pixel-by-pixel analysis of DCE MRI curve patterns and an illustration of its application to the imaging of the musculoskeletal system. Magn Reson Imaging 25:604–612

Lebon V, Carlier PG, Brillault-Salvat C, Leroy-Willig A (1998a) Simultaneous measurement of perfusion and oxygenation changes using a multiple gradient-echo sequence: application to human muscle study. Magn Reson Imaging 16:721–729

Lebon V, Bloch G, Leroy-Willig A, Carlier PG, Brillault-Salvat C (1998b) Evidence of muscle BOLD effect revealed by simultaneous interleaved gradient-echo NMRI and myoglobin NMRS during leg ischemia. Magn Reson Med 40:551–558

Lebon VPG, Brillault-Salvat C, Bloch G, Leroy-Willig AC (1998c) Anisotropy of the BOLD effect in the skeletal muscle. In: Proceedings ISMRM Sydney 1424

Ledermann HP et al (2006a) Calf muscles imaged at BOLD MR: correlation with TcPO2 and flowmetry measurements during ischemia and reactive hyperemia–initial experience. Radiology 241:477–484

Ledermann HP et al (2006b) Blood oxygenation level-dependent magnetic resonance imaging of the skeletal muscle in patients with peripheral arterial occlusive disease. Circulation 113:2929–2935

Leng GC, Fowkes FG, Allan PL, Ruckley CV (1991) Doppler colour flow imaging in peripheral arterial disease. Br J Hosp Med 45:200, 202, 204–207

Leppek R et al (2004) MR-Imaging of lower leg muscle perfusion. Herz 29:32–46

Loerakker S et al (2011) Ischemia-reperfusion injury in rat skeletal muscle assessed with T2-weighted and dynamic contrast-enhanced MRI. Magn Reson Med 66:528–537

Logothetis NK, Wandell BA (2004) Interpreting the BOLD signal. Annu Rev Physiol 66:735–769

Luh WM, Wong EC, Bandettini PA, Hyde JS (1999) QUIPSS II with thin-slice TI1 periodic saturation: a method for improving accuracy of quantitative perfusion imaging using pulsed arterial spin labeling. Magn Reson Med 41:1246–1254

Luo Y et al (2002) Evaluation of tissue perfusion in a rat model of hind-limb muscle ischemia using dynamic contrast-enhanced magnetic resonance imaging. J Magn Reson Imaging 16:277–283

Lutz AM et al (2004) Assessment of skeletal muscle perfusion by contrast medium first-pass magnetic resonance imaging: technical feasibility and preliminary experience in healthy volunteers. J Magn Reson Imaging 20:111–121

MacDonald ME, Smith MR, Frayne R (2011) Deconvolution with simple extrapolation for improved cerebral blood flow measurement in dynamic susceptibility contrast magnetic resonance imaging during acute ischemic stroke. Magn Reson Imaging 29:620–629

Mai VM, Berr SS (1999) MR perfusion imaging of pulmonary parenchyma using pulsed arterial spin labeling techniques: FAIRER and FAIR. J Magn Reson Imaging 9:483–487

Marcovecchio ML, Chiarelli F (2011) Microvascular disease in children and adolescents with type 1 diabetes and obesity. Pediatr Nephrol (Berlin, Germany) 26:365–375

Marro K (1997) FAWSETS: flow-driven arterial water stimulation with elimination of tissue signal. J Magn Reson (San Diego, CA: 1997) 124:240–244

Marro KI, Hyyti OM, Vincent MA, Kushmerick MJ (2005a) Validation and advantages of FAWSETS perfusion measurements in skeletal muscle. NMR Biomed 18:226–234

Marro KI, Hyyti OM, Kushmerick MJ (2005b) FAWSETS perfusion measurements in exercising skeletal muscle. NMR Biomed 18:322–330

Mattila KT, Komu ME, Koskinen SK, Niemi PT (1993) Exercise-induced changes in magnetization transfer contrast of muscles. Acta Radiol (Stockholm, Sweden: 1987) 34:559–562

Mattila KT, Komu ME, Dahlström S, Koskinen SK, Heikkilä J (1999) Medial tibial pain: a dynamic contrast-enhanced MRI study. Magn Reson Imaging 17:947–954

Mayr NA et al (1996) Tumor perfusion studies using fast magnetic resonance imaging technique in advanced cervical cancer: a new noninvasive predictive assay. Int J Radiat Oncol Biol Phys 36:623–633

Mayr NA et al (2000) Pixel analysis of MR perfusion imaging in predicting radiation therapy outcome in cervical cancer. J Magn Reson Imaging 12:1027–1033

Ménard JC, Giacomini E, Baligand C, Fromes Y, Carlier PG (2010) Non-invasive and quantitative evaluation of peripheral vascular resistances in rats by combined NMR measurements of perfusion and blood pressure using ASL and dynamic angiography. NMR Biomed 23:188–195

Meyer RA et al (2004) BOLD MRI mapping of transient hyperemia in skeletal muscle after single contractions. NMR Biomed 17:392–398

Muller-Delp JM (2006) Aging-induced adaptations of microvascular reactivity. Microcirculation 13:301–314

Niemi PT, Komu ME, Koskinen SK (1992) Tissue specificity of low-field-strength magnetization transfer contrast imaging. J Magn Reson Imaging 2:197–201

Norris DG, Schwarzbauer C (1999) Velocity selective radiofrequency pulse trains. J Magn Reson (San Diego, CA: 1997) 137:231–236

Noseworthy MD, Kim JK, Stainsby JA, Stanisz GJ, Wright GA (1999) Tracking oxygen effects on MR signal in blood and skeletal muscle during hyperoxia exposure. J Magn Reson Imaging 9:814–820

Noseworthy MD, Bulte DP, Alfonsi J (2003) BOLD magnetic resonance imaging of skeletal muscle. Semin Musculoskelet Radiol 7:307–315

Noseworthy MD, Davis AD, Elzibak AH (2010) Advanced MR imaging techniques for skeletal muscle evaluation. Semin Musculoskelet Radiol 14:257–268

Nygren AT, Greitz D, Kaijser L (2000) Skeletal muscle perfusion during exercise using Gd-DTPA bolus detection. J Cardiovasc Magn Reson 2:263–270

O'Connor JPB et al (2011) Dynamic contrast-enhanced imaging techniques: CT and MRI. Br J Radiol 84:S112–S120

Ogawa S, Lee TM, Nayak AS, Glynn P (1990a) Oxygenation-sensitive contrast in magnetic resonance image of rodent brain at high magnetic fields. Magn Reson Med 14:68–78

Ogawa S, Lee TM, Kay AR, Tank DW (1990b) Brain magnetic resonance imaging with contrast dependent on blood oxygenation. Proc Natl Acad Sci USA 87:9868–9872

Ogawa S et al (1992) Intrinsic signal changes accompanying sensory stimulation: functional brain mapping with magnetic resonance imaging. Proc Natl Acad Sci USA 89:5951–5955

Pack NA, DiBella EVR (2010) Comparison of myocardial perfusion estimates from dynamic contrast-enhanced magnetic resonance imaging with four quantitative analysis methods. Magn Reson Med 64:125–137

Panting JR et al (2002) Abnormal subendocardial perfusion in cardiac syndrome X detected by cardiovascular magnetic resonance imaging. N Engl J Med 346:1948–1953

Partovi S et al (2012a) Effects of covert and overt paradigms in clinical language fMRI. Acad Radiol 19:518–525

Partovi S et al (2012b) Clinical implications of skeletal muscle blood-oxygenation-level-dependent (BOLD) MRI. Magma New York NY. doi:10.1007/s10334-012-0306-y

Partovi S et al (2012c) Blood oxygenation level-dependent (BOLD) MRI of human skeletal muscle at 1.5 and 3 T. J Magn Reson Imaging 35:1227–1232

Partovi S et al (2012d) Impaired skeletal muscle microcirculation in systemic sclerosis. Arthritis Res Ther 14:R209

Partovi S et al (2012e) Clinical standardized fMRI reveals altered language lateralization in brain tumor patients. Am J Neuroradiol 1–7. doi:10.3174/ajnr.A3137

Partovi S et al (2013) Correlation of muscle BOLD MRI with transcutaneous oxygen pressure for assessing microcirculation in patients with systemic sclerosis. J Magn Reson Imaging. doi: 10.1002/jmri.24046. (Epub ahead of print)

Pedersen BK, Akerstrom TC, Nielsen AR, Fischer CP (2007) Role of myokines in exercise and metabolism. J Appl Physiol 103:1093–1098

Picchi A et al (2010) Coronary microvascular dysfunction in diabetes mellitus: a review. World J Cardiol 2:377–390

Pollak AW et al (2012) Arterial spin labeling MR imaging reproducibly measures peak-exercise calf muscle perfusion: a study in patients with peripheral arterial disease and healthy volunteers. JACC Cardiovasc Imaging 5:1224–1230

Potthast S, Schulte A, Kos S, Aschwanden M, Bilecen D (2009) Blood oxygenation level-dependent MRI of the skeletal muscle during ischemia in patients with peripheral arterial occlusive disease. Rofo 181:1157–1161

Prince MR (1998) Peripheral vascular MR angiography: the time has come. Radiology 206:592–593

Proctor DN, Koch DW, Newcomer SC, Le KU, Leuenberger UA (2003) Impaired leg vasodilation during dynamic exercise in healthy older women. J Appl Physiol 95:1963–1970

Quarles CC, Gore JC, Xu L, Yankeelov TE (2012) Comparison of dual-echo DSC-MRI- and DCE-MRI-derived contrast agent kinetic parameters. Magn Reson Imaging 30:944–953

Ranft J, Heidrich H, Peters A, Trampisch H (1986) Laser-Doppler examinations in persons with healthy vasculature and in patients with peripheral arterial occlusive disease. Angiology 37:818–827

Raynaud JS et al (2001) Determination of skeletal muscle perfusion using arterial spin labeling NMRI: validation by comparison with venous occlusion plethysmography. Magn Reson Med 46:305–311

Rehwald WG, Chen E-L, Kim RJ, Judd RM (2004) Noninvasive cineangiography by magnetic resonance global coherent free precession. Nat Med 10:545–549

Richardson RS, Haseler LJ, Nygren AT, Bluml S, Frank LR (2001) Local perfusion and metabolic demand during exercise: a noninvasive MRI method of assessment. J Appl Physiol (Bethesda, MD: 1985) 91:1845–1853

Rieber A et al (2002) Breast MRI for monitoring response of primary breast cancer to neo-adjuvant chemotherapy. Eur Radiol 12:1711–1719

Rissanen TT et al (2005) Blood flow remodels growing vasculature during vascular endothelial growth factor gene therapy and determines between capillary arterialization and sprouting angiogenesis. Circulation 112:3937–3946

Robson PM et al (2012) Imaging of renal masses: correlation with Histopathologic. 265:799–808

Rofsky NM, Adelman MA (2000) MR angiography in the evaluation of atherosclerotic peripheral vascular disease. Radiology 214:325–338

Saeed M (2001) New concepts in characterization of ischemically injured myocardium by MRI. Exp Biol Med (Maywood, NJ) 226:367–376

Sanchez OA, Copenhaver EA, Elder CP, Damon BM (2010) Absence of a significant extravascular contribution to the skeletal muscle BOLD effect at 3 T. Magn Reson Med 64:527–535

Sanchez OA et al (2011) Postmaximal contraction blood volume responses are blunted in obese and type 2 diabetic subjects in a muscle-specific manner. Am J Physiol 301:H418–H427

Sarelius I, Pohl U (2010) Control of muscle blood flow during exercise: local factors and integrative mechanisms. Acta Physiol (Oxf) 199:349–365

Schraml C, Schwenzer NF, Martirosian P, Claussen CD, Schick F (2011) Temporal course of perfusion in human masseter muscle during isometric contraction assessed by arterial spin labeling at 3T. Magma (New York, NY) 24:201–209

Schulte AC, Speck O, Oesterle C, Hennig J (2001) Separation and quantification of perfusion and BOLD effects by simultaneous acquisition of functional I(0)- and T2(*)-parameter maps. Magn Reson Med 45:811–816

Schulte AC, Aschwanden M, Bilecen D (2008) Calf muscles at blood oxygen level-dependent MR imaging: aging effects at postocclusive reactive hyperemia. Radiology 247:482–489

Schwarzbauer C, Morrissey SP, Haase A (1996) Quantitative magnetic resonance imaging of perfusion using magnetic labeling of water proton spins within the detection slice. Magn Reson Med 35:540–546

Silva AC, Kim SG (1999) Pseudo-continuous arterial spin labeling technique for measuring CBF dynamics with high temporal resolution. Magn Reson Med 42:425–429

Slade JM, Towse TF, Gossain VV, Meyer RA (2011) Peripheral microvascular response to muscle contraction is unaltered by early diabetes but decreases with age. J Appl Physiol (Bethesda, MD: 1985) 111, 1361–1371

Slagsvold C-E, Stranden E, Rosen L, Kroese AJ (1992) The role of blood perfusion and tissue oxygenation in the postischemic transcutaneous pO2 response. Angiology 43:155–162

Speck O, Hennig J (1998) Functional imaging by I0- and T2*-parameter mapping using multi-image EPI. Magn Reson Med 40:243–248

Talagala SL, Barbier EL, Williams DS, Silva AC, Koretsky AP (1998) Multi-slice perfusion MRI using continuous arterial water labeling: controling for MT effects with simultaneous proximal and distal RF irradiation. In: Proceedings of the 6th annual meeting of ISMRM 381. http://cds.ismrm.org/ismrm-1998/PDF2/p0381.pdf

Themen F (1997) Methodische Ansätze zur quantitativen Beurteilung der Mikrozirkulation im Gewebe mit der dynamischen. Radiologe 37: 470–480

Thompson RB et al (2005) Measurement of skeletal muscle perfusion during postischemic reactive hyperemia using contrast-enhanced MRI with a step-input function. Magn Reson Med 54:289–298

Thulborn KR, Waterton JC, Matthews PM, Radda GK (1982) Oxygenation dependence of the transverse relaxation time of water protons in whole blood at high field. Biochim Biophys Acta 714:265–270

Tofts PS et al (1999) Estimating kinetic parameters from dynamic contrast-enhanced T(1)-weighted MRI of a diffusable tracer: standardized quantities and symbols. J Magn Reson Imaging 10:223–232

Toussaint JF et al (1996) Perfusion changes in human skeletal muscle during reactive hyperemia measured by echo-planar imaging. Magn Reson Med 35:62–69

Towse TF, Slade JM, Meyer RA (2005) Effect of physical activity on MRI-measured blood oxygen level-dependent transients in skeletal muscle after brief contractions. J Appl Physiol 99:715–722

Towse TF, Slade JM, Ambrose JA, Delano MC, Meyer RA (2011) Quantitative analysis of the post-contractile blood-oxygenation-level-dependent (BOLD) effect in skeletal muscle. J Appl Physiol 111:27–39

Troalen T, Capron T, Cozzone PJ, Bernard M, Kober F (2013) Cine-ASL: a steady-pulsed arterial spin labeling method for myocardial perfusion mapping in mice. Part I. Experimental study. Magn Reson Med. doi:10.1002/mrm.24565

Turner R (1997) Signal sources in bold contrast fMRI. Adv Exp Med Biol 413:19–25

Utz W et al (2005) Blood oxygen level-dependent MRI of tissue oxygenation: relation to endothelium-dependent and endothelium-independent blood flow changes. Arterioscler Thromb Vasc Biol 25:1408–1413

Van der Leij C, van de Sande MGH, Lavini C, Tak PP, Maas M (2009) Rheumatoid synovial inflammation: pixel-by-pixel dynamic contrast-enhanced MR imaging time-intensity curve shape analysis – a feasibility study. Radiology 253:234–240

Van der Woude HJ et al (1998) Musculoskeletal tumors: does fast dynamic contrast-enhanced subtraction MR imaging contribute to the characterization? Radiology 208:821–828

Van der Zwaag W et al (2009) fMRI at 1.5, 3 and 7 T: characterising BOLD signal changes. Neuroimage 47:1425–1434

Van Rijswijk CS, Hogendoorn PC, Taminiau AH, Bloem JL (2001) Synovial sarcoma: dynamic contrast-enhanced MR imaging features. Skeletal Radiol 30:25–30

Versluis B et al (2011) Magnetic resonance imaging in peripheral arterial disease: reproducibility of the assessment of morphological and functional vascular status. Invest Radiol 46:11–24

Versluis B et al (2012) Dynamic contrast-enhanced MRI assessment of hyperemic fractional microvascular blood plasma volume in peripheral arterial disease: initial findings. PLoS ONE 7:e37756

Verstraete KL et al (1994) Benign and malignant musculoskeletal lesions: dynamic contrast-enhanced MR imaging–parametric "first-pass" images depict tissue vascularization and perfusion. Radiology 192:835–843

Vonken EP, van Osch MJ, Bakker CJ, Viergever MA (2000) Simultaneous quantitative cerebral perfusion and Gd-DTPA extravasation measurement with dual-echo dynamic susceptibility contrast MRI. Magn Reson Med 43:820–827

Walker UA et al (2007) Clinical risk assessment of organ manifestations in systemic sclerosis: a report from the EULAR Scleroderma trials and research group database. Ann Rheum Dis 66:754–763

Van de Sande MGH et al (2012) Characteristics of synovial inflammation in early arthritis analysed by pixel-by-pixel time-intensity curve shape analysis. Rheumatology (Oxford, England) 51:1240–1245

Wang DJJ et al (2012) The value of arterial spin-labeled perfusion imaging in acute ischemic stroke: comparison with dynamic susceptibility contrast-enhanced MRI. Stroke 43:1018–1024

Weber M-A, Kroll A, Günther M (2004) Noninvasive measurement of relative cerebral blood flow using arterial spin labeling techniques: physical basics and clinical applications. Radiologe 44:164–173

Weber MA, Risse F, Giesel FL, Schad LR, Kauczor HU, Essig M (2005) Measurement of perfusion using the first-pass dynamic susceptibility-weight ed contrast-enhanced (DSC) MRI in neuro-oncology. Physical basics and clinical applications. Radiologe 45:618–632

Weber MA, Krix M, Delorme S (2007) Quantitative evaluation of muscle perfusion with CEUS and with MR. Eur Radiol 17:2663–2674

Wheaton AJ, Miyazaki M (2012) Non-contrast enhanced MR angiography: physical principles. J Magn Reson Imaging 36:286–304

Wigmore DM, Damon BM, Pober DM, Kent-Braun JA (2004) MRI measures of perfusion-related changes in human skeletal muscle

during progressive contractions. J Appl Physiol (Bethesda, MD: 1985) 97:2385–2394

Wong EC, Buxton RB, Frank LR (1998) A theoretical and experimental comparison of continuous and pulsed arterial spin labeling techniques for quantitative perfusion imaging. Magn Reson Med 40:348–355

Wong EC et al (2006) Velocity-selective arterial spin labeling. Magn Reson Med 55:1334–1341

Wu W-C, Fernández-Seara M, Detre JA, Wehrli FW, Wang J (2007) A theoretical and experimental investigation of the tagging efficiency of pseudocontinuous arterial spin labeling. Magn Reson Med 58:1020–1027

Wu W-C, Wang J, Detre JA, Ratcliffe SJ, Floyd TF (2008) Transit delay and flow quantification in muscle with continuous arterial spin labeling perfusion-MRI. J Magn Reson Imaging 28:445–452

Wu W-C et al (2009) Skeletal muscle microvascular flow in progressive peripheral artery disease: assessment with continuous arterial spin-labeling perfusion magnetic resonance imaging. J Am Coll Cardiol 53:2372–2377

Wu W, Lawrence KSS, Licht DJ, Wang DJJ (2011) Quantification issues in arterial spin labeling perfusion. 21:65–73

Yankeelov TE, Gore JC (2009) Dynamic contrast enhanced magnetic resonance imaging in oncology: theory, data acquisition, analysis, and examples. Curr Med Imaging Rev 3:91–107

Ye FQ, Frank JA, Weinberger DR, McLaughlin AC (2000) Noise reduction in 3D perfusion imaging by attenuating the static signal in arterial spin tagging (ASSIST). Magn Reson Med 44:92–100

Yeung DKW, Griffith JF, Li AFW, Ma HT, Yuan J (2012) Air pressure-induced susceptibility changes in vascular reactivity studies using BOLD MRI. J Magn Reson Imaging. doi: 10.1002/jmri.23926

Zhang H et al (2005) Accurate myocardial T1 measurements: toward quantification of myocardial blood flow with arterial spin labeling. Magn Reson Med 53:1135–1142

Zhu XP, Zhao S, Isherwood I (1992) Magnetization transfer contrast (MTC) imaging of skeletal muscle at 0.26 Tesla–changes in signal intensity following exercise. Br J Radiol 65:39–43

Zierath JR, Hawley JA (2004) Skeletal muscle fiber type: influence on contractile and metabolic properties. PLoS Biol 2:e348

Ziv K et al (2004) Longitudinal MRI tracking of the angiogenic response to hind limb ischemic injury in the mouse. Magn Reson Med 51:304–311